

Propagated α -synucleinopathy recapitulates REM sleep behaviour disorder followed by parkinsonian phenotypes in mice

Yan Shen,^{1,†} Wen-Bo Yu,^{1,†} Bo Shen,^{1,†}  Hui Dong,² Jue Zhao,¹ Yi-Lin Tang,¹ Yun Fan,¹ Yan-Fei Yang,² Yi-Min Sun,¹ Su-Shan Luo,¹ Chen Chen,¹ Feng-Tao Liu,¹ Jian-Jun Wu,¹ Bao-Guo Xiao,¹ Huan Yu,¹ James B. Koprach,^{1,3,‡}  Zhi-Li Huang^{1,2,‡} and  Jian Wang^{1,‡}

^{†,‡}These authors contributed equally to this work.

Idiopathic rapid eye movement sleep behaviour disorder (RBD) is now recognized as an early manifestation of α -synucleinopathies. Increasing experimental studies demonstrate that manipulative lesion or inactivation of the neurons within the sublaterodorsal tegmental nucleus (also known as the subcoeruleus nucleus in humans) can induce RBD-like behaviours in animals. As current RBD animal models are not established on the basis of α -synucleinopathy, they do not represent the pathological substrate of idiopathic RBD and thus cannot model the phenoconversion to Parkinson's disease. The purpose of this study was therefore to establish an α -synucleinopathy-based RBD animal model with the potential to convert to parkinsonian disorder. To this end, we first determined the functional neuroanatomical location of the sublaterodorsal tegmental nucleus in wild-type C57BL/6J mice and then validated its function by recapitulating RBD-like behaviours based on this determined nucleus. Next, we injected preformed α -synuclein fibrils into the sublaterodorsal tegmental nucleus and performed regular polysomnographic recordings and parkinsonian behavioural and histopathological studies in these mice. As a result, we recapitulated RBD-like behaviours in the mice and further showed that the α -synucleinopathy and neuron degeneration identified within the sublaterodorsal tegmental nucleus acted as the neuropathological substrates. Subsequent parkinsonian behavioural studies indicated that the α -synucleinopathy-based RBD mouse model were not stationary, but could further progress to display parkinsonian locomotor dysfunction, depression-like disorder, olfactory dysfunction and gastrointestinal dysmotility. Corresponding to that, we determined α -synuclein pathology in the substantia nigra pars compacta, olfactory bulb, enteral neuroplexus and dorsal motor nucleus of vagus nerve, which could underlie the parkinsonian manifestations in mice. In conclusion, we established a novel α -synucleinopathy-based RBD mouse model and further demonstrated the phenoconversion of RBD to Parkinson's disease in this animal model.

- 1 Department of Neurology and National Research Center for Aging and Medicine, State Key Laboratory of Medical Neurobiology, Huashan Hospital, Fudan University, Shanghai, China
- 2 Department of Pharmacology, School of Basic Medical Sciences, State Key Laboratory of Medical Neurobiology and MOE Frontiers Center for Brain Science, Institutes of Brain Science, Fudan University, Shanghai, China
- 3 Krembil Institute, Toronto Western Hospital, University Health Network, Toronto, ON M5T 2S8, Canada

Correspondence to: Dr Jian Wang
Department of Neurology and National Research Center for Aging and Medicine, Huashan Hospital, Fudan University, Shanghai 200040, China
E-mail: wangjian336@hotmail.com

Correspondence may also be addressed to: Dr Zhi-Li Huang
E-mail: huangzli@fudan.edu.cn

Received March 10, 2020. Revised June 18, 2020. Accepted July 12, 2020.

© The Author(s) (2020). Published by Oxford University Press on behalf of the Guarantors of Brain. All rights reserved.
For permissions, please email: journals.permissions@oup.com

Dr James B. Koprich
 Krembil Institute, Toronto Western Hospital, University Health Network, Toronto, ON M5T
 2S8, Canada
 E-mail: j.koprich@atuka.com

Keywords: α -synucleinopathy; sublateralodorsal tegmental nucleus; rapid eye movement sleep behaviour disorder; Parkinson's disease; preformed α -synuclein fibrils

Abbreviations: AAV = adeno-associated virus; m.p.i. = months post injection; PFF = preformed α -synuclein fibril; RBD = rapid eye movement sleep behaviour disorder; REM = rapid eye movement; RWA = rapid eye movement sleep without atonia; SLD = sublateralodorsal tegmental nucleus; SNc = substantia nigra pars compacta; SWS = slow wave sleep

Introduction

Rapid eye movement (REM) sleep (also referred to as paradoxical sleep) is a specific sleep stage characterized by theta wave predominant cortical activation and generalized skeletal muscle atonia (Dement and Kleitman, 1957; Peever and Fuller, 2017). REM sleep behaviour disorder (RBD) is a parasomnia featured by a loss of skeletal muscle atonia and an excess of tonic/phasic muscle twitches during REM sleep (Dauvilliers et al., 2018), which usually drives the patients to act out the ongoing dream scenarios. Since the first clinical description of RBD in humans (Schenck et al., 1986), several longitudinal follow-up studies report that 73.5–92.5% of idiopathic RBD patients can develop α -synucleinopathies including Parkinson's disease, multiple system atrophy (MSA) and dementia with Lewy bodies (DLB) within 10–14 years (Schenck et al., 1996, 2013; Iranzo et al., 2013, 2014; Postuma et al., 2019). Post-mortem studies on idiopathic RBD patients identify α -synuclein pathology and neuronal loss in multiple brainstem structures, which includes the REM sleep modulating nuclei such as subcoeruleus nucleus and magnocellular reticular nucleus (Uchiyama et al., 1995; Turner et al., 2000; Boeve et al., 2007a). Based on this evidence, idiopathic RBD is recognized as an early manifestation of α -synucleinopathies (Hogel et al., 2018), with the REM sleep circuit-based neurodegeneration acting as the pathological substrates (Boeve, 2013; Peever et al., 2014; McKenna and Peever, 2017).

In light of the long prodromal period and high conversion ratio to α -synucleinopathies (Boeve, 2013; Dauvilliers et al., 2018), RBD is deemed as more than an isolated clinical syndrome, but rather represents an early disease-modifying time window for the neurodegenerative disease (Weil and Morris, 2019). Thus, further clarification of the underlying neuropathogenic mechanisms of RBD and its subsequent conversion to α -synucleinopathies would be of great significance. To achieve this goal, it is a prerequisite to establish an animal model that can mimic the phenotypic and neuropathological features of idiopathic RBD. Since the discovery that mechanical lesions to cat pontine tegmentum can lead to violent dream-enactment behaviours during REM sleep (Jouvet, 1962), the sleep researchers gradually focused on this area and demonstrated that sublateralodorsal tegmental nucleus (SLD, also known as the subcoeruleus nucleus in humans) is

crucial for the maintenance of muscle atonia during REM sleep (REM atonia) (Lu et al., 2006; Fuller et al., 2007; Fort et al., 2009; Luppi et al., 2011). Based on this premise, neurotoxic lesion (Lu et al., 2006) and genetic silencing (Krenzer et al., 2011; Valencia Garcia et al., 2017, 2018) methods were used to degenerate or incapacitate the neurons within SLD and induced RBD-like behaviours in experimental animals. However, these RBD animal models are established based on manipulative breakdown of the REM sleep circuit, and thus neither represent the α -synuclein pathology substrate of idiopathic RBD nor mimic the phenocopy of RBD to Parkinson's disease (Peever et al., 2014; McKenna and Peever, 2017). Hence, establishing a novel SLD-based RBD animal model with α -synuclein pathology substrate and neurodegeneration-inducing potential would be of great significance.

In recent years, preformed α -synuclein fibrils (PFFs) are proven to be able to seed the formation of Lewy-body like inclusions by recruiting and converting endogenous soluble α -synuclein protein into insoluble pathological aggregates (Luk et al., 2009; Volpicelli-Daley et al., 2014). Moreover, PFFs can initiate neuron-to-neuron transmission of α -synuclein pathology *in vivo* by binding lymphocyte-activation gene 3 (LAG3) (Mao et al., 2016). Concomitant with the α -synuclein pathology transmission are cytoplasmic inclusion formation, neuronal cell death (Desplats et al., 2009) and Parkinson's disease-like neurodegeneration (Luk et al., 2012a). For example, two recent studies report that a single injection of PFFs into mouse olfactory bulb (Rey et al., 2016) or enteral muscular layer (Kim et al., 2019) can induce not only local neuron degeneration but also widespread propagation of α -synucleinopathy. In line with the neuropathological substrates, the mice develop progressive olfactory deficits, gastrointestinal dysmotility and other parkinsonian behavioural dysfunctions (Rey et al., 2016; Kim et al., 2019), which further corroborates the potential of PFFs in inducing α -synucleinopathy and neurodegeneration.

Based on these study findings and observations, we hypothesized that injection of PFFs into mouse SLD could induce local neuron degeneration and widespread propagation of α -synuclein pathology, which could further recapitulate RBD-like behaviours followed by parkinsonian phenotypes in mice. We tested this hypothesis by a combination of polysomnographic recording, parkinsonian

behavioural testing and neuropathological validation, and demonstrated that (i) the injection of PFFs into SLD could establish an α -synucleinopathy-based RBD mouse model; and (ii) this RBD mouse model was not stationary, but could further progress to develop parkinsonian behavioural and histopathological phenotypes. This novel animal model could not only help to unravel the mechanisms behind the initiation and phenoconversion of RBD, but could also be utilized to develop or screen the disease-modifying therapeutics for Parkinson's disease in future studies.

Materials and methods

Animals

The specific-pathogen-free (SPF) C57BL/6J male mice (2-months-old, 18–20 g) were purchased from Shanghai Laboratory Animal Center, Chinese Academy of Science (SLAC, Shanghai, China) and housed four to five per cage under a constant temperature ($22 \pm 0.5^\circ\text{C}$), humidity ($55 \pm 5\%$) and an automatically controlled 12-h light/12-h dark cycle (lights on at 7 a.m., illumination intensity ≈ 100 lx), with access to food and water *ad libitum*. All the animal husbandry and related procedures were performed in accordance with the institutional guidelines and approved by the Animal Care and Use Committee of Fudan University.

Preparation and characterization of preformed fibrils

Recombinant full-length human monomeric α -synuclein proteins (specially formulated to generate PFFs) were purchased from Proteos (RP-003) and stored at -80°C for use. In accordance with previously established protocols (Volpicelli-Daley *et al.*, 2014), we synthesized the PFFs by continuously shaking α -synuclein monomers in an Eppendorf orbital thermomixer (1000 rpm, 37°C) for 7 days (Supplementary Fig. 1). Then we determined the endotoxin level (EU/ml) and identified that it was within permitted ranges (< 0.5 EU/ml). After the sonication treatment (2 s on/off, 100 s in total, 10% amplitude; Zollo Digital Sonifier), the concentration of PFFs was determined by BCA protein assay method and the final concentration was adjusted to 5 mg/ml.

We used the Thioflavin T (ThT) assay and transmission electron microscopy (TEM, Tecnai G2 Spirit Biotwin) to characterize the fibrillar morphology (phosphotungstic acid negative staining; Supplementary Fig. 2A–C) and amyloid β -sheet structure (Supplementary Fig. 2D) of PFFs, respectively. As fibril fragmentation is proven to enhance cytotoxicity (Xue *et al.*, 2009), we further determined the fibril number and length within nine TEM scanning fields and identified that the mean fibril length was 27.8 ± 1.2 nm. Based on the TEM study findings, we revealed that most majority (84.77%) of the fibrils used in the study were ≤ 50 nm (Supplementary Fig. 2E).

Stereotaxic injections

All surgical procedures were performed in accordance with aseptic technique. The mice were anaesthetized with isoflurane/

oxygen mixture (2–3%) and kept at constant body temperature with a heating cushion. After scalp preparation and antisepsis, the mice were mounted on stereotaxic head frame (RWD Life Science) and small holes (1 mm in diameter) above the target nuclei were drilled on the skull. The pulled glass micropipettes (~ 30 μm tip diameter), preloaded with viruses, sterile PBS or PFFs, were gradually descended into target nuclei and then connected to an air pressure propelling apparatus (Picospritzer III, Parker Hannifin Corp.) to inject the inoculum (virus, PBS or PFFs) into target nuclei (infusion speed = 5 nl/min).

The following coordinates used for microinjection were based on the Mouse Brain Atlas of Paxinos and Franklin (Franklin and Paxinos, 2013): (i) to retrogradely label the SLD neurons, we injected the AAV2/retro-hSyn-eGFP (70 nl per injection) and AAV2/retro-CMV_bGI-Cre-eGFP (70 nl per injection) into bilateral ventral gigantocellular reticular nucleus (AP/ML/DV: $-6.72 \pm 0.25/-5.60$ mm); (ii) to induce the selective apoptosis of SLD neurons, we injected the AAV2/9-CAG-DIO-taCaspase 3 (100 nl per injection) into bilateral mouse SLD (AP/ML/DV: $-5.20 \pm 0.75/-4.10$ mm). Identical volumes of virus diluent were injected as the control; (iii) to initiate α -synuclein pathology in the SLD, PFFs were first premixed with AAV2/9-hSyn-mCherry (200 nl PFFs plus 20 nl site-reporting virus per injection) and then injected into bilateral SLD (AP/ML/DV: $-5.20 \pm 0.75/-4.10$ mm). The same volumes of sterile PBS were injected as the control. After the infusions, the pipettes were kept *in situ* for 10 min and then withdrawn slowly. Following the injections, the mice were sutured and caged individually to recover for 1 week.

EEG/EMG electrodes implantation

The mice were first anaesthetized with isoflurane/oxygen mixture (2–3%). After scalp preparation, antisepsis and fixation on the stereotaxic holder, two small holes (1 mm in diameter) were drilled epidurally on the frontal (AP/ML: $+1.50/-0.80$ mm) and parietal (AP/ML: $-1.50/-1.00$ mm) bone surface. As indicated by a previous study (Zhang *et al.*, 2017), the EEG/EMG recording electrode is composed of two stainless steel screws (1 mm in diameter) and two Teflon-coated silver leads (0.2 mm in diameter), with the former acting as the EEG electrodes and the latter as EMG electrodes. During the process of electrodes implantation surgery, the EEG electrodes were screwed into the frontal and parietal bone holes, and the EMG electrodes were inserted into bilateral trapezius muscle. The EEG and EMG electrodes were connected to a mini-connector to form an electrode assembly, which were then fixed on the skull surface with dental base acrylic resin. After the surgery, the mice were individually caged and allowed 7 days to recover before the video-polysomnography recordings.

Video-polysomnography recording

The mice were first connected to the sleep recording equipment to habituate for 72 h before the formal video-polysomnography recordings. The cortical EEG and nuchal EMG signals, digitized at a sampling rate of 512 Hz, were firstly amplified, filtered (Biotex) and then recorded by the CED 1401 digitizer plus Spike 2 software (CED, UK). Then the Spike 2 data were converted to visualizable vigilance states by the SleepSign software (Kissei Comtec, Japan). The animal behaviour monitoring system were synchronous with the polysomnography recording equipment.

REM sleep deprivation and rebound

The mice dedicated to the SLD location determination experiment were implanted with EEG/EMG recording electrodes in advance and then submitted to the REM sleep deprivation (RSD, 72 h) and rebound (RSR, 3 h) procedures with standard flower-pot method (Clement *et al.*, 2011; Valencia Garcia *et al.*, 2017, 2018), which spanned from 12 a.m. on Day 1 to 3 p.m. on Day 3. Before the experiment, the mice were randomly divided into two subgroups: (i) RSD group mice were placed on the stainless-steel platforms (3 cm in diameter) in a transparent barrel (four platforms in total, surrounded by water of 3.5 cm in depth) at 12 a.m. (Day 1), receiving continuous REM sleep deprivation for 75 h; (ii) RSD/RSR group mice were first submitted to the REM sleep deprivation protocol for 72 h and then allowed 3 h to recover in the home cage. During the REM sleep deprivation and rebound processes, food and water were available to all mice *ad libitum* and the vigilance states of both mouse groups were recorded with polysomnography. After the REM sleep deprivation and rebound procedures, all the mice were sacrificed within 30 min to collect the brains for histological studies.

Polysomnographic data analysis

Vigilance state parameter analysis

The mouse vigilance states (scored by 4 s per epoch) were automatically classified into wake, REM sleep and slow wave sleep (SWS, also known as non-REM sleep) by the SleepSign software. To highlight the RBD attack episodes, we defined the REM epoch with motor behaviours (confirmed by synchronous video) as the 'M' epoch. These automatically defined wake, REM and SWS were then manually checked and corrected in case of incompatibility. If RBD behaviours occurred in specific REM sleep episodes, relevant REM episodes would be defined as 'M' (REM sleep with motor behaviours) in the hypnogram. Following manual proofreading and correction, the quantity, percentage, transition and duration of each vigilance state were calculated.

EMG signal quantification

Based on previous study protocols (Valencia Garcia *et al.*, 2017, 2018), we used the MATLAB (Mathworks, USA) to quantify the nuchal muscle tone intensity and then determine the mean EMG value during REM and SWS episodes (EMG_{REM} and EMG_{SWS}). To avoid the vigilance stage transition (e.g. SWS-REM-SWS or SWS-REM-Wake) induced muscle tone alterations, we only included the REM episodes that lasted more than 48 s and eliminated the foremost and last 8 s during the quantification processes.

EEG spectral analysis

By utilizing the fast Fourier transform (FFT) analysis module integrated into the SleepSign software, we first extracted the EEG frequency spectral data from this software. Then, we used the MATLAB to transform the raw frequency data into an EEG spectrogram based on the standard EEG rhythms (delta: 0.65–4 Hz, theta: 6–10 Hz, alpha: 12–14 Hz, beta: 15–25 Hz) (Zhang *et al.*, 2017). Hypnograms were simultaneously exported to match the EEG spectrogram.

Behavioural tests

Before the behavioural tests, the mice were allowed 1 h to habituate to the testing room. The experimental instruments were

cleaned with 75% ethanol after each trial to minimize odour cues. All the tests were performed by one experimenter who was blinded to the treatment group classification. Apart from the faecal output assay, all the other behavioural tests were performed between 7 p.m. and 12 p.m. in the light-off period. To minimize the light influence on the animal's sleep-wake cycle and nocturnal behaviours, we used red-light illumination in the testing room and controlled the light intensity below 10 lx (Zhang *et al.*, 2017).

Rotarod test

We used the Rotarod test to assess the parkinsonian locomotor dysfunction in mice. The test lasted for three consecutive days. On Days 1 and 2, each mouse was trained to acclimate to the testing apparatus (Med-Associates). The training protocol was as follows: running on a constantly accelerating rod (4 to 40 rpm within 5 min) for five trials, 10 min apart. On Day 3, the same protocol was performed and the latency (in seconds) to fall off the rod was recorded. The mean latency time of the five trials was calculated for each mouse.

Tail suspension test

We used the tail suspension test to assess the depression-like disorder in mice. The mice were suspended in a Plexiglas box (black wall, 50 × 50 × 50 cm), with tail tips (1.5 cm from tail end) securely fastening to a stable rod with medical adhesive tape and hanging 5 cm above the box floor. For each mouse, the test time lasted for 6 min. After eliminating the first 2 min, the percentage of immobility time was computed with the ANY-maze software (Stoelting, USA). Immobility was defined as an absence of limb and trunk movements, simultaneously without body centre displacement.

Buried food pellets test

We used the buried food pellets test to evaluate the odour detection ability of mice (Kim *et al.*, 2019). Before the formal testing, mice were deprived of food supply for 24 h (7 p.m., Day 1 to 7 p.m., Day 2), but with free access to water. During the period of food restriction, weights and vital signs of each mouse were closely monitored. On the testing day, the mice were placed in a clean transparent PVC cage (46 cm long × 23.5 cm wide × 20 cm high) in advance, filled with 3-cm deep fresh woodchips, to acclimatize to the testing surroundings for 20 min. After the acclimation, the bedding was changed and a piece of standard mouse chow (1 g, Xietong Organism, China) was randomly buried 1 cm below the bedding. Then the mice were placed in the cage and the latency to find the food pellet was recorded. After finding the food pellets, the mice were allowed to consume it. The upper limit of the testing time was 5 min. The timing end point was defined as touching the food pellet by nose or forelimbs. After each trial, the cage was cleaned with ethanol and the bedding was changed to minimize odour cues.

Food/water intake and faecal output assay

We used the food/water intake and faecal output assay to evaluate the gastrointestinal motility function in mice (Kim *et al.*, 2019). Before the test, the body weight of each mouse was measured. Then the mice were transferred to a clean cage (without woodchip bedding) and housed individually for 24 h (spanning from 7 a.m., Day 1 to 7 a.m., Day 2), with free access to food and water. During the testing period, the faecal pellets of

each mouse were collected every 2 h. After the test, we first determined the pellet number and wet weight of the faecal pellets from each mouse. Then the faecal samples were thoroughly oven-dried (80°C, 24 h) and weighed again to calculate the faecal water percentage with the following equation: faecal water percentage (%) = [(wet weight – dry weight)/wet weight] × 100%.

Animal sacrifice and frozen sectioning

The mice were anaesthetized with over-dosed sodium pentobarbital (100 mg/kg, intraperitoneally) and transcardially perfused with ice-cold PBS. For the striatal monoamine neurotransmitter determination study, the mouse striata were immediately dissected on ice and stored at –80°C. For the histopathological studies, the mouse brain and colon were collected and post-fixed for 24 h in 4% paraformaldehyde (4%, pH 7.4), followed by a gradient dehydration in sucrose/PBS solutions (4°C, 10%, 20%, 30%, pH 7.4). Next, the mouse brain and colons were rapidly frozen with OCT embedding compound (Sakura) and serially sectioned with a cryostat microtome (Leica). The serial brain (30 µm) and colon sections (8 µm) were collected and classified into six identical batches (six series) for use.

High performance liquid chromatography

As previously described (Luk *et al.*, 2012a), we used high performance liquid chromatography (HPLC) to determine the concentration of striatal monoamine neurotransmitter and its metabolites. Briefly, the mouse striatum was first weighed and homogenized in 0.2 M perchloric acid solution containing 100 µM EDTA (4°C). The homogenates were centrifuged (15 000g, 30 min, 4°C) and then mixed with 1 M sodium acetate (1:2, vol/vol) to adjust the pH to 3.0. After centrifugal filtration with a 0.22 µm membrane, 20 µl supernatant was pipetted to inject into the HPLC system and determined by an electrochemical detector (Waters). The chromatograms were recorded and analysed with the Millennium 32 Chromatography Manager Software (Waters, Milford, MA, USA).

Histopathological studies

Immunofluorescence analysis

The antibodies and working solutions used are detailed in [Supplementary Tables 1 and 2](#). Free-floating sections were firstly blocked with 10% normal donkey serum (Jackson ImmunoResearch, 30 min, 20°C) and then incubated in PBST (0.3% TritonTM X-100 in PBS) containing rabbit IgG against c-fos (1:10 000, Millipore) for 72 h at 4°C. After washing with PBS, the sections were then incubated in PBST containing Alexa Fluor[®] 568 conjugated donkey anti-rabbit IgG (1:1000, Invitrogen) for 2 h at room temperature. After DAPI counterstaining (1:200, Sigma-Aldrich), the sections were mounted onto slides and cover-slipped with Antifade Mounting Medium (Vectorshield HardsetTM, Vector Laboratories). Finally, the fluorescence images were captured by an Olympus confocal microscope (Olympus Confocal LSM FV3000) and processed with the offline Olympus Fluoview Software (v. 4.2b).

Immunohistochemistry and stereoscopic analysis

The antibodies and working solutions used are detailed in [Supplementary Table 1 and 2](#). First, the sections were sequentially blocked with 5% H₂O₂ and 10% normal goat or horse serum (Vector Laboratories) at 20°C for 30 min. After washing with PBS, the sections were incubated in PBST containing rabbit IgG against tyrosine hydroxylase (TH, 1:1000, Abcam), rabbit IgG against p- α -synuclein^{Ser129} (1:500, Abcam) or mouse IgG against neuronal nuclear antigen (NeuN, 1:1000, Abcam) overnight at 4°C. Then the sections were incubated with biotinylated goat-anti-rabbit IgG or biotinylated horse anti-mouse IgG (1:1000, Vector Laboratories) at 20°C for 2 h. After the avidin-biotin (1:1000, ABC Elite Kit, Vector Laboratories) incubation, the sections were revealed with 3,3'-diaminobenzidine (DAB, Vector Laboratories) as the chromogen. Following the counterstaining with Cresyl violet (Beyotime) or haematoxylin (Vector Laboratories), images were captured by the DP74 digital camera connected to an Olympus microscope (Olympus).

Stereoscopic quantification of the TH-, NeuN- and pS129- α -synuclein-positive neurons in substantia nigra pars compacta (SNc, 1:6 series) and SLD (1:6 series) were determined by the Stereo Investigator System (Micro Bright Field Bioscience). The striatal fibre density was assessed with the mean optical density (OD) value on three representative coronal sections (AP: +0.98 mm, +0.74 mm and +0.14 mm) by using ImageJ software (NIH, USA).

Spatiotemporal distribution and quantitative analysis of the α -synucleinopathy

To assess the spatiotemporal distribution of α -synucleinopathy in mice receiving PFF injection, we first performed immunohistochemical staining of pS129- α -synuclein on the mouse brain sections at 1, 3, 5 and 8 months post injection (m.p.i.). Then we plotted a schematic brain map to trace all the pS129- α -synuclein immunoreactive neuronal inclusions and neurites (indicated by dots and curves, respectively) on nine representative coronal sections (AP +3.92, +2.96, +0.62, –1.82, –3.00, –5.20, –5.52, –6.64 and –7.64 mm) from 1, 3, 5 to 8 m.p.i.

On these coronal sections, we quantified the pS129- α -synuclein positive cells within olfactory bulb, striatum, amygdala, hippocampus, SNc, SLD, locus coeruleus and dorsal motor nucleus of vagus nerve using ImageJ software. As previously described (Kim *et al.*, 2019), we determined the α -synucleinopathy density by calculating the average pS129- α -synuclein immunoreactive cell numbers per square millimetre within these nuclei, and the data are presented as pS129- α -synuclein-positive cells/mm².

Post-mortem clinicopathological study on a patient with Parkinson's disease

Based on the BRISQ (Biospecimen Reporting for Improved Study Quality) guidelines (Moore *et al.*, 2011), we sampled the patient tissue from representative central and peripheral anatomical sites including olfactory bulb, striatum, amygdala, hippocampus (CA1), SNc, subcoeruleus nucleus, locus coeruleus, dorsal motor nucleus of vagus nerve and descending colon ([Supplementary Table 3](#)). Following the fixation, gradient dehydration, cryotome sectioning, pS129- α -synuclein

immunostaining and haematoxylin counterstaining, images of the sections were captured (DP74, Olympus) and assembled to form montages (Photoshop CS6, Adobe System, USA).

The patient tissue samples were obtained from the Body Donation Station in Fudan University (Shanghai Red Cross Society), which was in accordance with the institutional ethical standards as laid down in the 1964 Declaration of Helsinki. The patient's clinical data including the rating scales, questionnaires and ^{18}F -FDG PET/CT images were extracted from Huashan Parkinson's Disease Patient Follow-up Cohort Database. Ethical approval was granted by Huashan Hospital Ethics Committee and the informed consent was obtained from this patient and her close relatives.

Statistical analysis

All data were processed and analysed with Microsoft Excel (Microsoft Corporation, Redmond, WA, USA) and GraphPad Prism 8 software (GraphPad prism, San Diego, CA, USA). Statistical differences between groups were assessed using independent sample Student's *t*-test, one-way or two-way ANOVA followed by Bonferroni's *post hoc* multiple comparison analysis. Box-and-whisker plots show the means (plus sign), the 25th, 50th and 75th percentiles, minima and maxima; *n* represents the number of animals used in respective experimental tests. The relevance between neuronal quantities and animal behaviours was determined using the Pearson's correlation analysis. Statistical significance was indicated when $P < 0.05$.

Data availability

The data that support the findings of this study are available from the corresponding author upon reasonable request.

Results

Determination of the functional neuroanatomic location of SLD in mouse pontine tegmentum

As previous works in relation to the SLD are mostly performed in cats (Jouvet, 1962) and rats (Lu *et al.*, 2006; Valencia Garcia *et al.*, 2017), we therefore first determined the functional neuroanatomical location of SLD in mice (Supplementary Fig. 3) by the joint use of tract-tracing and flower-pot methods (Clement *et al.*, 2011; Valencia Garcia *et al.*, 2017, 2018) in the present study. As shown in Supplementary Fig. 3A and B, the adeno-associated virus (AAV) was first injected into mouse ventral gigantocellular reticular nucleus, which retrogradely labelled the pontine tegmentum with GFP [Supplementary Fig. 3E(i, ii, vi and vii)]. After a significant rebound of REM sleep ($11.17 \pm 1.36\%$, $P < 0.0001$, $t = 7.397$, $df = 11$; Supplementary Fig. 3C and D), mice in the RSD/R group ($n = 7$) showed an elevated expression of *c-fos*, a marker for neuron activation, in pontine tegmentum [Supplementary Figs 3E(viii), 4C and H]. Based on the distribution ranges of the GFP- and *c-fos* double-positive neurons in pontine

tegmentum [Supplementary Figs 3E(vi–x), 4D and I], we determined the functional neuroanatomical location of SLD [Supplementary Figs 3E(v and x), 4E and J] and identified that the most predominant co-localization section was located at AP -5.20 mm relative to the bregma [Supplementary Fig. 3E(iv, v, ix and x)].

Selective apoptosis of the neurons within the determined SLD nucleus induces RBD-like behaviours in mice

To validate the function of the SLD nucleus determined in this study, we used the Cre-loxP system-based viruses to induce selective neuron apoptosis within SLD and then monitored the animal sleep/wake behaviours with the video-polysomnography (Fig. 1A and B). As shown in Fig. 1C, we first retrogradely labelled the SLD neuron subpopulations with GFP and Cre-recombinase from the downstream ventral gigantocellular nucleus. Then we used the Cre-recombinase-dependent AAV2/9-FLEX-Caspase 3 virus to selectively exterminate the GFP and Cre labelled SLD neurons (Fig. 1D). As a result, mice in the Caspase 3 group ($n = 8$) displayed a 52.3% loss (756.8 ± 55.72 versus 1588 ± 58.13 , Caspase 3 versus mice in the control group) of the NeuN (neuronal nuclear antigen, a mature neuronal marker) positive neurons when compared with the control counterparts ($n = 8$) ($P < 0.0001$, unpaired two-tailed Student's *t*-test, $t = 10.33$, $df = 14$; Fig. 1E–G).

We next scrutinized the video-polysomnography recording data and identified that mice in the control group presented a sustained low muscle tone intensity during REM sleep (Fig. 2A and Supplementary Video 4). In contrast, mice in the Caspase 3 group displayed frequent myoelectric bursts (indicated by arrows on EMG waveform, Fig. 2B) and elevated background muscle tone intensity (EMG_{REM} , $2000 \mu\text{V}$ versus $500 \mu\text{V}$, Caspase 3 versus control group; Fig. 2B). In line with the electromyographic features, violent leaping, pawing and scratching behaviours were identified in the Caspase 3 group by the time-locked video monitoring system, which repeatedly discontinued the REM sleep and induced frequent wake from sleep (Supplementary Videos 1–3). Additionally, compared with the control group ($n = 8$), a significantly increased REM episode number ($P = 0.0006$, $t = 4.372$, $df = 14$; Fig. 2C), decreased REM episode duration ($P = 0.0005$, $t = 4.531$, $df = 14$; Fig. 2D), higher percentage of 'M' phases (REM episodes with motor behaviours) ($P < 0.0001$, $t = 6.873$, $df = 14$; Fig. 2E) and more REM-to-wake transitions [$F(1,56) = 5.360$, $P = 0.0243$; Supplementary Fig. 5B] were revealed in the Caspase 3 group ($n = 8$). However, statistical comparison of the wake and sleep percentage between mice in the Caspase 3 and control groups showed no difference (Supplementary Fig. 5A). Together, these data suggested that selective neuron apoptosis within SLD could induce violent RBD-like behaviours, which frequently discontinued the REM episodes and thus contributed to REM sleep 'fragmentation' in mice.

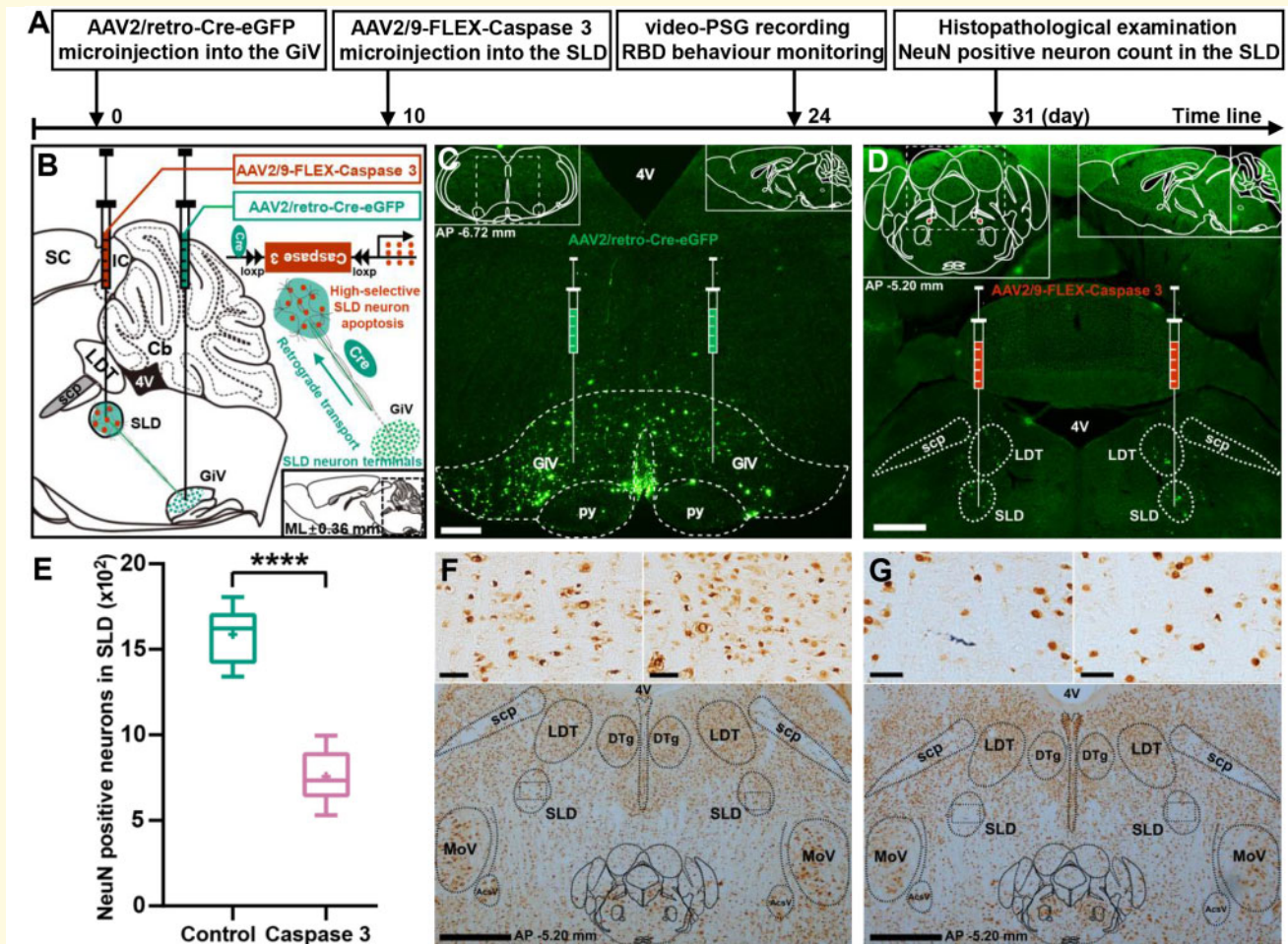


Figure 1 Cre-loxP system-based viral vectors injection induces selective neuron apoptosis within the SLD nucleus in mice. (A) Experimental flow chart. (B) Schematic diagram of the selective neuron apoptosis strategy, with AAV2/retro-Cre-eGFP and AAV2/9-FLEX-Caspase 3 viruses respectively injected into the ventral gigantocellular nucleus and SLD. In the presence of Cre-recombinase, the reversed Caspase 3 gene elements flanked by the loxP sites will be inverted and then induce neuron apoptosis within the SLD nucleus. (C and D) Photomicrographs showing the virus injection sites in the ventral gigantocellular nucleus (C, AP -6.72 mm) and SLD (D, AP -5.20 mm). Scale bars = 100 μ m in C; 500 μ m in D. (E) Statistical comparison of the NeuN positive neuron count in the SLD between control ($n = 8$) and Caspase 3 group ($n = 8$) mice. (F and G) Representative photomicrographs showing NeuN immunostaining in the pontine tegmentum (AP -5.20 mm) of a control (F) and a Caspase 3 (G) group mouse. The insets are a higher magnification of the rectangular areas in the SLD. Scale bars = 500 μ m in F and G; 40 μ m in the insets of F and G. Box-and-whisker plots (E) show the means (plus sign), median, the 25th and 75th percentiles, minima and maxima. Statistical significance was determined using the unpaired two-tailed Student's *t*-test. **** $P < 0.0001$. 4V = the fourth ventricle; AcsV = accessory trigeminal nucleus; Cb = cerebellum; Cre = Cre-recombinase; DTg = dorsal tegmental nucleus; FLEX = flip-excision; GiV = ventral gigantocellular reticular nucleus; IC = inferior colliculus; LDT = laterodorsal tegmental nucleus; MoV = motor trigeminal nucleus; NeuN = neuronal nuclear antigen; PSG = polysomnography; SC = superior colliculus; scp = superior cerebellar peduncle.

Previous studies indicate that the myoelectric bursts in RBD can be divided into two subtypes: phasic and tonic bursts (Lapierre and Montplaisir, 1992). In comparison with the phasic bursts, the tonic bursts are likely to result in continuous muscle tonus (Lapierre and Montplaisir, 1992). By manual scrutiny of the sleep recording videos, we could identify the RBD episodes with visible trunk or extremity movements, but failing to determine the RBD episodes that manifested as 'invisible' muscle tonus. Hence, to better characterize the RBD behaviours in mice, we determined the integral muscle tone intensity during REM and SWS sleep

(EMG_{REM} and EMG_{SWS}) and then compared that between Caspase 3 and control mouse groups (Fig. 2F and G). Compared with the 'plummeting' trend of $EMG_{SWS-REM}$ in controls ($n = 8$), mice in the Caspase 3 group ($n = 8$) displayed a flat or upward variation pattern of $EMG_{SWS-REM}$, accompanying significantly elevated EMG_{REM} level [$F(1,14) = 77.26$, $P < 0.0001$; Fig. 2F]. In line with this, the EMG_{REM}/EMG_{SWS} ratio of the Caspase 3 group ($n = 8$) surpassed the cut-off value of 1 and was significantly higher than that of control counterparts ($n = 8$, $P = 0.0004$, $t = 4.668$, $df = 14$; Fig. 2G). Collectively, these results

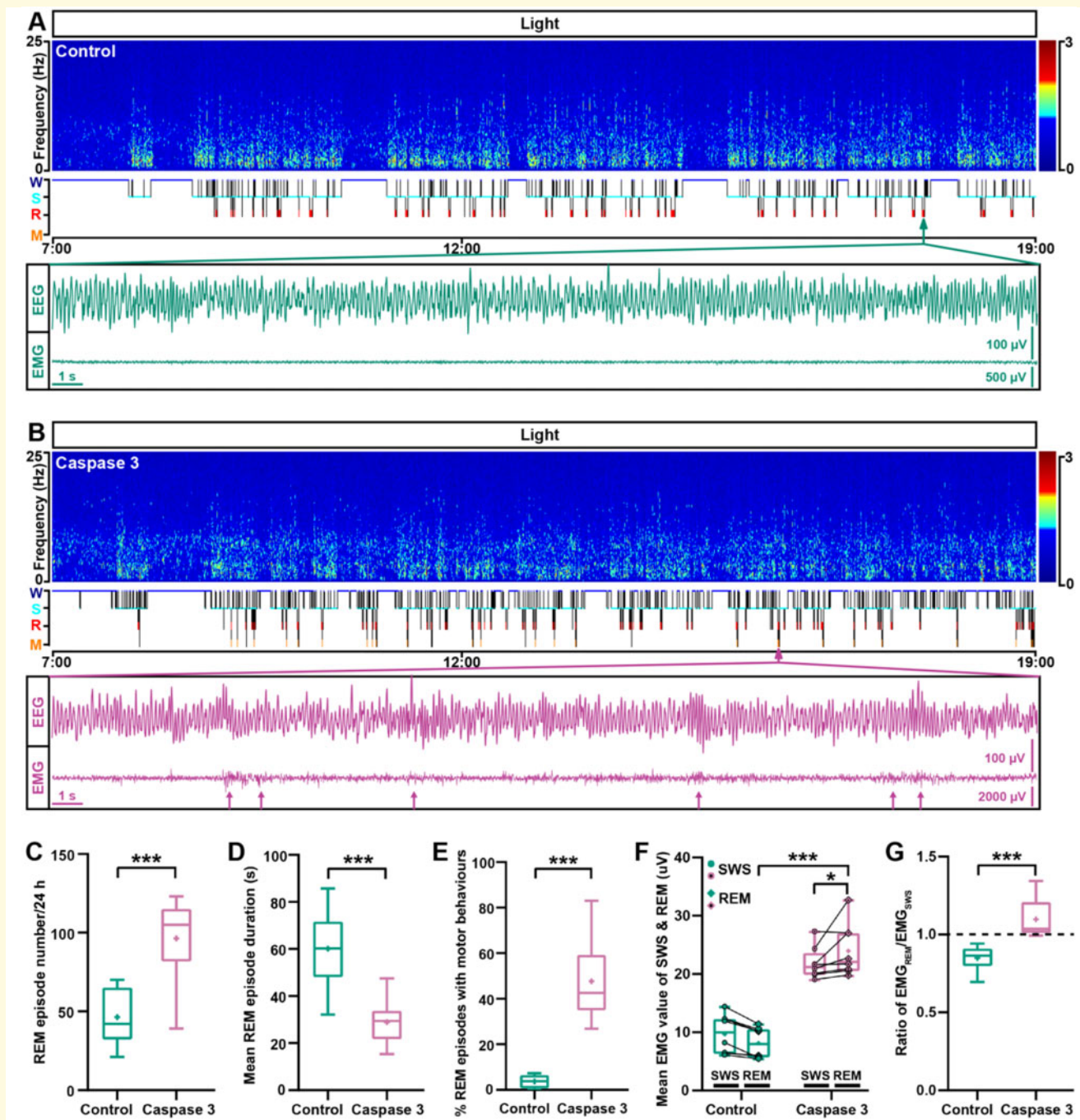


Figure 2 Selective neuron apoptosis within the determined SLD nucleus recapitulates frequent myoelectric activity and enhanced muscle tone intensity during REM sleep in mice. (A and B) Typical EEG power spectrograms (light period, 7:00–19:00; top), hypnograms (middle) and EEG and EMG waveforms (bottom) of control (A) and Caspase 3 group (B) mice. The 'M' phase was added to the hypnogram to represent the REM episodes with motor behaviours (B, middle). Myoelectric bursts during REM sleep were indicated by the red arrows on EMG waveform (B). (C–E and G) Statistical comparison of the REM episode number (C), mean REM episode duration (D), percentage of REM episodes with motor behaviours (E) and the ratio of EMG_{REM}/EMG_{SWS} (G) between mice in the control ($n = 8$) and Caspase 3 ($n = 8$) groups. (F) Quantification and comparison of the paired EMG_{SWS} (dots) and EMG_{REM} (rhombi) between mice in the control ($n = 8$) and Caspase 3 ($n = 8$) groups. Box-and-whisker plots show the means (plus sign), median, the 25th and 75th percentiles, minima and maxima. Statistical significance was determined using the unpaired two-tailed Student's *t*-test. The comparison of EMG_{REM} between mice in the control and Caspase 3 groups (F) used the repeated measure two-way ANOVA followed by Bonferroni's multiple comparison test. * $P < 0.05$, *** $P < 0.001$. M = REM episodes with motor behaviours; R = REM sleep; S = slow wave sleep (SWS); W = wake.

indicated that selective neuron apoptosis within SLD could compromise or reverse the REM atonia state and in turn resulted in enhanced muscle tone intensity during REM sleep in mice.

In conclusion, we validated the function of the SLD nucleus determined in this study and demonstrated that it was essential for the maintenance of REM atonia. Furthermore, our data indicated that selective neuron apoptosis within SLD could induce violent RBD-like behaviours, fragmented REM sleep structure and enhanced muscle tone intensity during REM sleep, which closely imitated the RBD behaviours in humans.

Injection of PFFs into the SLD nucleus recapitulates RBD-like behaviours in mice

We first premixed the PFFs or PBS with AAV2/9-hSyn (human synapsin 1)-mCherry and then injected it into the SLD at AP -5.20 mm (Supplementary Fig. 6A and B). With the mCherry expressed *in situ* acting as the injection site-reporting marker (Supplementary Fig. 6C, F and I), we proved that PFFs and PBS were injected into the SLD, which fully enveloped this nucleus from rostral to caudal sections and not intruded adjacent pontine nuclei (Supplementary Fig. 6D, G and J).

Following the injection, video-polysomnography recordings and histopathological studies were performed regularly at 1, 2 and 3 m.p.i. (Supplementary Fig. 7). We first used four parameters to assess the REM sleep architecture of the mice receiving PBS or PFFs injection (Supplementary Fig. 8). As a result, comparison of the REM sleep percentage [$F(2,37) = 2.170$, $P = 0.1285$; Supplementary Fig. 8A], REM episode number [$F(2,37) = 0.6335$, $P = 0.5364$; Supplementary Fig. 8B], mean REM episode duration [$F(2,37) = 0.2230$, $P = 0.8012$; Supplementary Fig. 8C] and vigilance stage transition number [$F(5,148) = 0.4679$, $P = 0.7997$; Supplementary Fig. 8D] between mice in the PBS ($n = 5, 5$ and 5 , respectively) and PFFs groups ($n = 10, 8$ and 10 , respectively) showed no statistical significance at 1, 2 and 3 m.p.i.

We then analysed the electromyographic features and motor behaviours during REM sleep (Fig. 3A–F). As shown in Fig. 3B, D and F, mice in the PFFs/1, 2 and 3 m.p.i. groups displayed frequent myoelectric bursts (indicated by arrows on EMG waveforms) during REM sleep. Time-locked videos corroborated that the PFFs group exhibited various RBD-like behaviours such as limb jerks, tail sweepings, forward leaping, etc., which implicated multiple body territories including whiskers, tail, nose, toes, head and limb extremities (Supplementary Videos 5–7). Statistical analysis of the motor behaviours indicated that the PFFs group ($n = 10, 8$ and 10) displayed significantly higher percentage of REM episodes with motor events [$F(1,7) = 77.46$, $P < 0.0001$] than that of control counterparts ($n = 5, 5$ and

5) at 1, 2 and 3 m.p.i. time points (Fig. 3G). Together, these data suggested that PFF injection could induce the mice to display frequent myoelectric activities and motor behaviours during REM episodes, but not altering the REM sleep architecture.

We next quantified the muscle tone intensity during SWS and REM sleep (EMG_{SWS} and EMG_{REM}) and then compared it between PBS and PFFs group mice. We observed similar results to the SLD neuron apoptosis study (Fig. 2F): the typical ‘plummeting’ trend of $EMG_{SWS-REM}$ disappeared in the PFFs group, and was replaced by a ‘flat or upward’ pattern (Fig. 3H). Statistical comparison of the mean EMG_{REM} between the PBS ($n = 5, 5$ and 5) and PFFs ($n = 10, 8$ and 10) groups showed significant differences at 1 m.p.i. [$F(1,13) = 8.890$, $P = 0.0106$], 2 m.p.i. [$F(1,11) = 19.83$, $P = 0.0010$] and 3 m.p.i. [$F(1,13) = 22.64$, $P = 0.0004$] (Fig. 3H and Supplementary Fig. 9). The EMG_{REM}/EMG_{SWS} ratio of the PFFs group mice ($n = 10, 8$ and 10) were also significantly higher [$F(1,37) = 87.59$, $P < 0.0001$] than that of control counterparts ($n = 5, 5$ and 5), at 1, 2 or 3 m.p.i. time points (Fig. 3I). Collectively, these data indicated that the injection of PFFs into SLD resulted in enhanced EMG_{REM} , which could underlie the frequent myoelectric activities and motor behaviours during REM episodes in mice.

α -Synucleinopathy and neuron degeneration identified within the SLD underlie the RBD-like behaviours in mice

To clarify the histopathological basis of the RBD-like behaviours in mice, we determined the neuron loss and α -synuclein pathology within the SLD nucleus. Compared with control mice ($n = 5, 5$ and 5 ; Fig. 4A and I), mice in the PFFs group ($n = 6, 8$ and 6) displayed significant NeuN positive neuron loss in the SLD from 2 to 3 m.p.i. [$F(2,29) = 19.40$, $P < 0.0001$], with about 1/3 (29.06%) of the total neurons being depleted at 3 m.p.i. (Fig. 4C, E, G and I). On the contrary, stereological quantification of pS129- α -synuclein-positive neurons in the SLD of the PFFs group mice ($n = 6, 8$ and 6) revealed a time-dependent increasing trend from 1 to 3 m.p.i. [$F(1,29) = 625.8$, $P < 0.0001$], which was significantly higher than that of control counterparts ($n = 5, 5$ and 5) at all the three time points [$F(2,29) = 30.56$, $P < 0.0001$; Fig. 4B, D, F, H and J]. The α -synuclein aggregates identified within the SLD nucleus gradually developed from sporadic immunoreactive freckles at 1 m.p.i. to dense cytoplasmic inclusions at 3 m.p.i., eventually encroaching the whole neuronal somas and neurites (Fig. 4D, F and H, arrows). Additionally, we demonstrated that there was a significant negative correlation between the SLD neuron quantities and the RBD behaviours in the PFFs group mice ($r = -0.8785$, $P < 0.001$, $n = 20$; Supplementary Fig. 10D). Taken together, these study data suggested that the α -

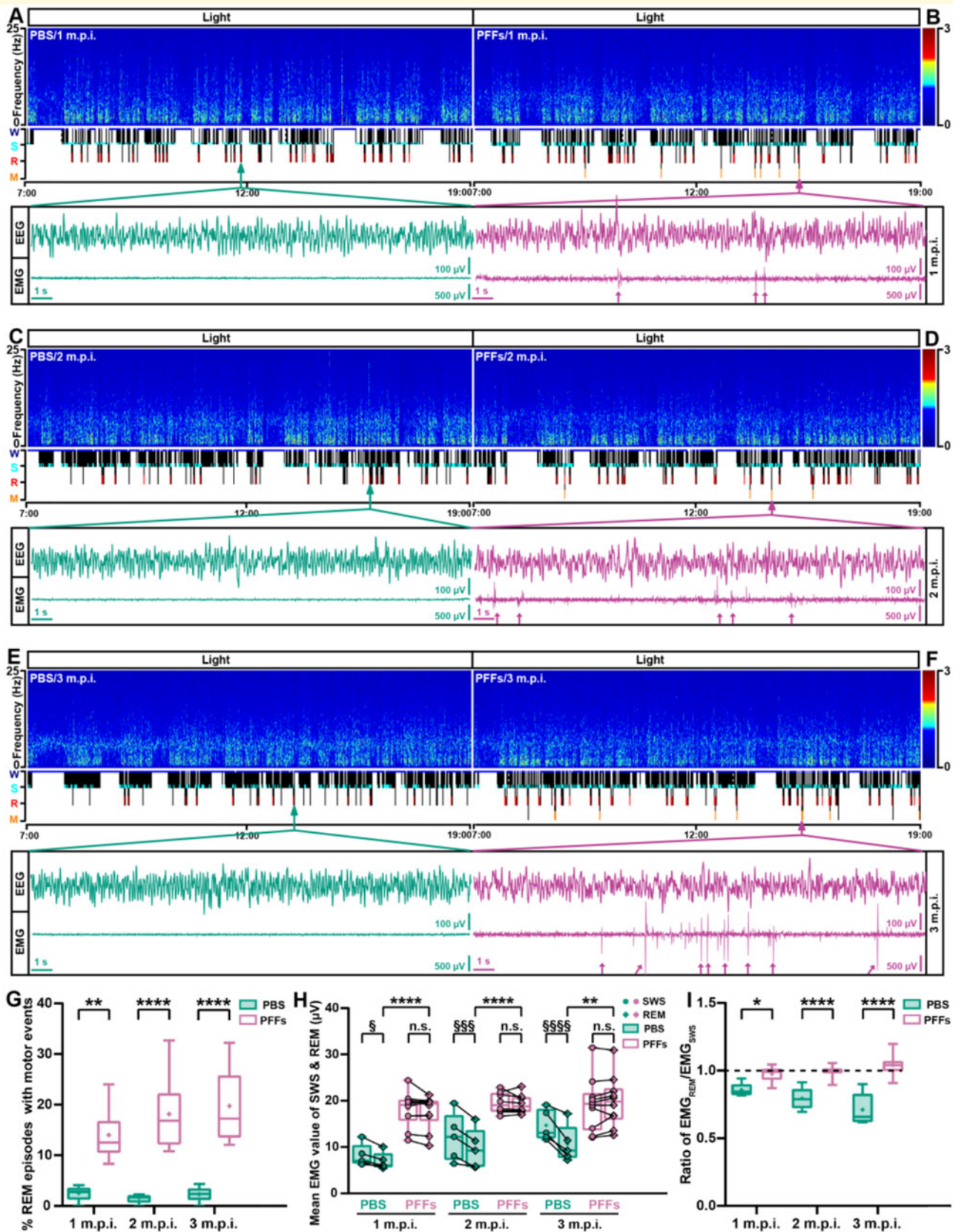


Figure 3 Injection of PFFs into the SLD nucleus induces frequent myoelectric activity and enhanced muscle tone intensity during REM sleep in mice. (A–F) Typical EEG power spectrograms (light period, 7:00–19:00; top), hypnograms (middle) and EEG and EMG waveforms (bottom) of mice in the PBS (A, C and E; 1, 2 and 3 m.p.i.) and PFFs (B, D and F; 1, 2 and 3 m.p.i.) groups. Myoelectric activities during REM sleep were indicated by the red arrows on EMG waveforms (B, D and F). (G and I) Statistical analysis of the percentage of REM episodes

(continued)

synucleinopathy and neuron degeneration identified within the SLD nucleus could underlie the RBD-like behaviours in mice.

RBD mice display progressive parkinsonian behavioural deficits and nigrostriatal degeneration

Previous studies suggest that pathological α -synuclein transmission can initiate Parkinson's disease-like neurodegeneration in mice (Luk *et al.*, 2012a; Kim *et al.*, 2019), we therefore investigated whether the α -synucleinopathy-based RBD mice could also progress to manifest parkinsonian behavioural and histopathological phenotypes (Supplementary Fig. 7). From 1, 3, 5 to 8 m.p.i., mice in the PFFs group ($n = 10, 10, 10$ and 20) displayed continuously decreased fall-off latency in Rotarod test [$F(1,68) = 71.08, P < 0.0001$; Fig. 5A], increased immobility time in tail suspension test [$F(1,68) = 33.20, P < 0.0001$; Fig. 5B] and prolonged food identification latency in olfaction test [$F(1,68) = 49.37, P < 0.0001$; Fig. 7A]. Similarly, in the gastrointestinal motility test, the PFFs group ($n = 10, 10, 10$ and 20) showed a progressive decline of faecal pellet number [$F(1,68) = 18.38, P < 0.0001$] and faecal water percentage [$F(1,68) = 111.8, P < 0.0001$] from 1, 3 to 5 m.p.i., which reached a plateau at 8 m.p.i. (Fig. 7E and F). Statistical comparison of the food intake [$F(3,68) = 0.8818, P = 0.4550$] and water consumption [$F(3,68) = 4.407, P = 0.0680$] between PFFs ($n = 10, 10, 10$ and 20) and PBS mouse groups ($n = 5, 5, 8$ and 8) showed no difference (Fig. 7B and C), but significant weight loss was identified in the PFFs group ($n = 10, 10, 10$ and 20) at 8 m.p.i. [$F(3,68) = 17.57, P < 0.0001$; Fig. 7D]. These data implied that the α -synucleinopathy-based RBD mice were not stationary, but could progress to develop parkinsonian motor and non-motor behavioural deficits, including locomotor dysfunction, depression-like disorder, olfactory dysfunction, gastrointestinal dysmotility and weight loss.

We next determined the nigrostriatal dopaminergic integrity (Fig. 6A–G) and nigral α -synuclein pathology (Fig. 5C–S) in mice. Analysis of the nigral TH-positive neuron quantity [$F(1,37) = 124.6, P < 0.0001$; Fig. 6E], striatal dopaminergic fibre density [$F(1,37) = 352.6, P < 0.0001$; Fig. 6F] and striatal dopamine concentration [$F(1,37) = 120.6, P < 0.0001$; Fig. 6G] in the PFFs group mice ($n = 6, 6, 5$ and 7) revealed a significant and time-dependent

decrease from 1, 3, 5 to 8 m.p.i. Concomitant with the striatal dopamine depletion, we also identified a progressive reduction of DOPAC [3,4-dihydroxyphenylacetic acid; $F(1,37) = 62.33, P < 0.0001$] and homovanillic acid (HVA) [$F(1,37) = 39.52, P < 0.0001$] in the PFFs group ($n = 6, 6, 5$ and 7), whereas the norepinephrine [$F(1,37) = 0.3729, P = 0.5452$] and serotonin level [$F(1,37) = 1.052, P = 0.3117$] remained unchanged (Supplementary Fig. 11A–D). In comparison, the nigral pS129- α -synuclein pathology in the PFFs group mice ($n = 6, 6, 5$ and 7) showed a continuous increase from 1 m.p.i. and culminated at 5 m.p.i. [$F(1,37) = 860.8, P < 0.0001$; Fig. 5C, L, M, N, P, Q and R]. At 8 m.p.i., the nigral pathology decreased to a level that was comparable to that at 3 m.p.i., but still being significantly higher [$F(3,37) = 52.58, P < 0.0001$] than that of control counterparts ($n = 5, 5, 5$ and 6) (Fig. 5C, O and S). In addition, we also performed correlation analyses between nigral dopaminergic neuron quantity and locomotor performance (assessed by Rota-rod test) in the PFFs group (Supplementary Fig. 12A–E), which indicated that nigral dopaminergic neuron degeneration correlated positively with the locomotor dysfunction ($r = 0.9541, P < 0.001, n = 24$; Supplementary Fig. 12E). In line with previous PFF injection study findings (Luk *et al.*, 2012a, b; Kim *et al.*, 2019), these data suggested that the seeded nigral α -synuclein pathology could result in progressive nigrostriatal degeneration, which further contributed to the locomotor dysfunction in RBD mice.

Seeded α -synucleinopathy underlies the olfactory dysfunction and gastrointestinal dysmotility in mice

Apart from the SLD and SNc, we demonstrated that the PFF-seeded α -synucleinopathy could propagate diffusely and progressively to implicate a wide range of brain structures, which extended from the rostral olfactory bulb to caudal vagal nucleus (Supplementary Figs 13A and 14A–H) and even involved the peripheral enteric neuroplexus (Fig. 7S). As shown in Fig. 7, we identified pS129- α -synuclein immunoreactive neurons (indicated by arrows) in the mitral cell layer of olfactory bulb (Fig. 7I and J) and dorsal motor nucleus of vagus nerve (Fig. 7N–P). We further quantified the α -synuclein pathology density within these two brain structures and revealed a continuously increasing trend from 1, 3, 5 to 8 m.p.i. (Supplementary Fig. 13B), which was contrary to the animal behavioural performances in the

Figure 3 Continued

with motor behaviours (G) and the ratio of EMG_{REM}/EMG_{SWS} (I) between mice in the PBS ($n = 5, 5$ and 5) and PFFs ($n = 10, 8$ and 10) groups at 1, 2 and 3 m.p.i. (H) Quantification and comparison of the paired EMG_{SWS} (dots) and EMG_{REM} (rhombi) between PBS ($n = 5, 5$ and 5) and PFFs ($n = 10, 8$ and 10) groups at 1, 2 and 3 m.p.i., respectively. Box-and-whisker plots show the means (plus sign), median, the 25th and 75th percentiles, minima and maxima. Statistical significance was determined using two-way ANOVA followed by Bonferroni's multiple comparison test. * $P < 0.05$, ** $P < 0.01$, *** $P < 0.0001$. Statistical comparison of the EMG_{SWS} versus EMG_{REM} within PBS or PFFs groups (H) used the repeated measure two-way ANOVA followed by Bonferroni's multiple comparison test. $^{\S}P < 0.05$, $^{\S\S\S}P < 0.001$, $^{\S\S\S\S}P < 0.0001$, n.s. = not significant. M = REM episodes with motor behaviours; R = REM sleep; S = slow wave sleep (SWS); W = wake.

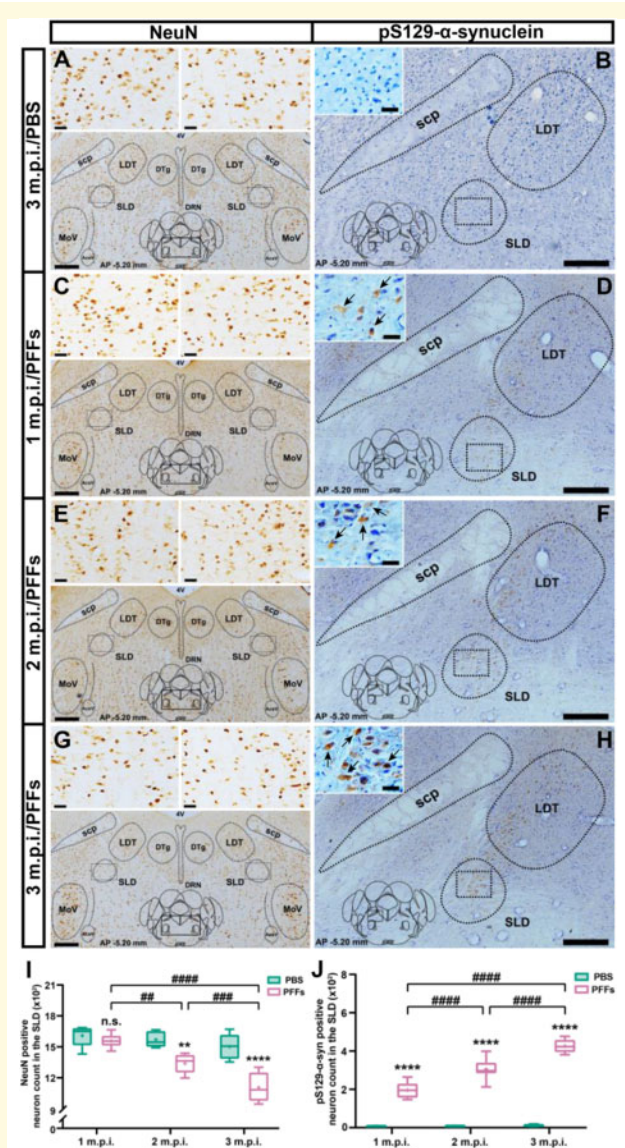


Figure 4 Progressive neuron degeneration and α -synuclein aggregation are identified within the SLD of PFFs group mice. (A–H) Representative photomicrographs showing the NeuN (A, C, E and G) and pS129- α -synuclein (B, D, F and H) immunostaining (indicated by arrows) on pontine tegmentum (containing the SLD nucleus) of PBS and PFFs group mice at 1, 2 and 3 m.p.i., respectively. The insets represented a higher magnification of the rectangular areas. (I and J) Quantification of the NeuN (I) and pS129- α -synuclein immunoreactive neurons (indicated by arrows, J) in the SLD of PBS ($n = 5, 5$ and 5) and PFFs ($n = 6, 8$ and 6) group mice at 1, 2 and 3 m.p.i., respectively. Scale bars = $300 \mu\text{m}$ in A, C, E and G; $200 \mu\text{m}$ in B, D, F and H; $30 \mu\text{m}$ in the insets of A–H. Box-and-whisker plots (I and J) show the means (plus sign), median, the 25th and 75th percentiles, minima and maxima. Statistical significance was determined using two-way ANOVA followed by Bonferroni's multiple comparison test. $**P < 0.01$, $***P < 0.0001$ versus PBS group; $###P < 0.01$, $####P < 0.001$, $#####P < 0.0001$, n.s. = not significant. AcsV = accessory trigeminal nucleus; DRN = dorsal raphe nucleus; DTg = dorsal tegmental nucleus; LDT = laterodorsal tegmental nucleus; MoV = motor trigeminal nucleus; NeuN = neuronal nuclear antigen; scp = superior cerebellar peduncle; 4V = the fourth ventricle.

olfaction test (Fig. 7A) and gastrointestinal motility assay (Fig. 7E and F). We also identified typical pS129- α -synuclein aggregates (indicated by arrows) within the submucosal (Fig. 7S and T) and myenteric plexuses (Fig. 7S, U and V) of mice in the PFFs group, which indicated a potential brain-to-gut transmission pattern of α -synucleinopathy (Ulusoy et al., 2017; Van Den Berge et al., 2019; Marie-Laure et al., 2020). These data collectively constituted the neuropathological basis of the olfactory dysfunction and gastrointestinal dysmotility in mice.

In addition, we performed post-mortem clinicopathological studies on a patient with Parkinson's disease, who had experienced RBD, hyposmia and constipation during the disease course (Supplementary Tables 4, 5 and Supplementary Fig. 15). Corresponding to the hyposmia and constipation, we identified typical Lewy bodies and Lewy neurites in the olfactory bulb (Supplementary Fig. 14I), dorsal motor nucleus of vagus nerve (Supplementary Fig. 14P) and enteric neuroplexuses (Fig. 7W–Z) of this patient. Similar to the α -synuclein pathology distribution patterns determined in the PFF-injected mice (Supplementary Figs 13A and 14A–H), we also identified Lewy pathology in a wide range of the patient's brain subregions (Supplementary Fig. 14I–P). Taken together, these animal and post-mortem study findings suggest that the PFF-seeded α -synuclein pathology in the olfactory bulb, vagal nucleus and enteric neuroplexuses could underlie the olfactory dysfunction and gastrointestinal dysmotility in mice.

Discussion

In this study, we introduced a novel α -synucleinopathy-based RBD modelling strategy in mice. In line with previous RBD animal models (Lu et al., 2006; Krenzer et al., 2011; Valencia Garcia et al., 2017), this model was also established based on SLD, a pivotal nucleus proven to be involved in the modulation of REM sleep and REM atonia (Lu et al., 2006; Fuller et al., 2007; Fort et al., 2009; Luppi et al., 2011; Peever and Fuller, 2017). As previous RBD modelling works in relation to SLD are mostly performed in cats (Jouvet, 1962) and rats (Lu et al., 2006; Valencia Garcia et al., 2017), the exact location of SLD in mice remained unclear. Though Krenzer et al. (2011) uses the retrograde tracing method to delineate the SLD location in mice, they only account for the anatomical connections between SLD and spinal ventral horn, which do not involve the ventral gigantocellular nucleus and not include the REM sleep-related functional parameters in the delineation process. Given this, we determined the functional neuroanatomical location of SLD in mice by the joint use of tract-tracing method (anatomical localization) and the flower-pot technique (functional localization) (Valencia Garcia et al., 2017, 2018). To confirm the SLD nucleus determined in this study was essential for the maintenance of REM atonia, we used the Cre-loxP system-based virus to induce selective neuron apoptosis within this nucleus

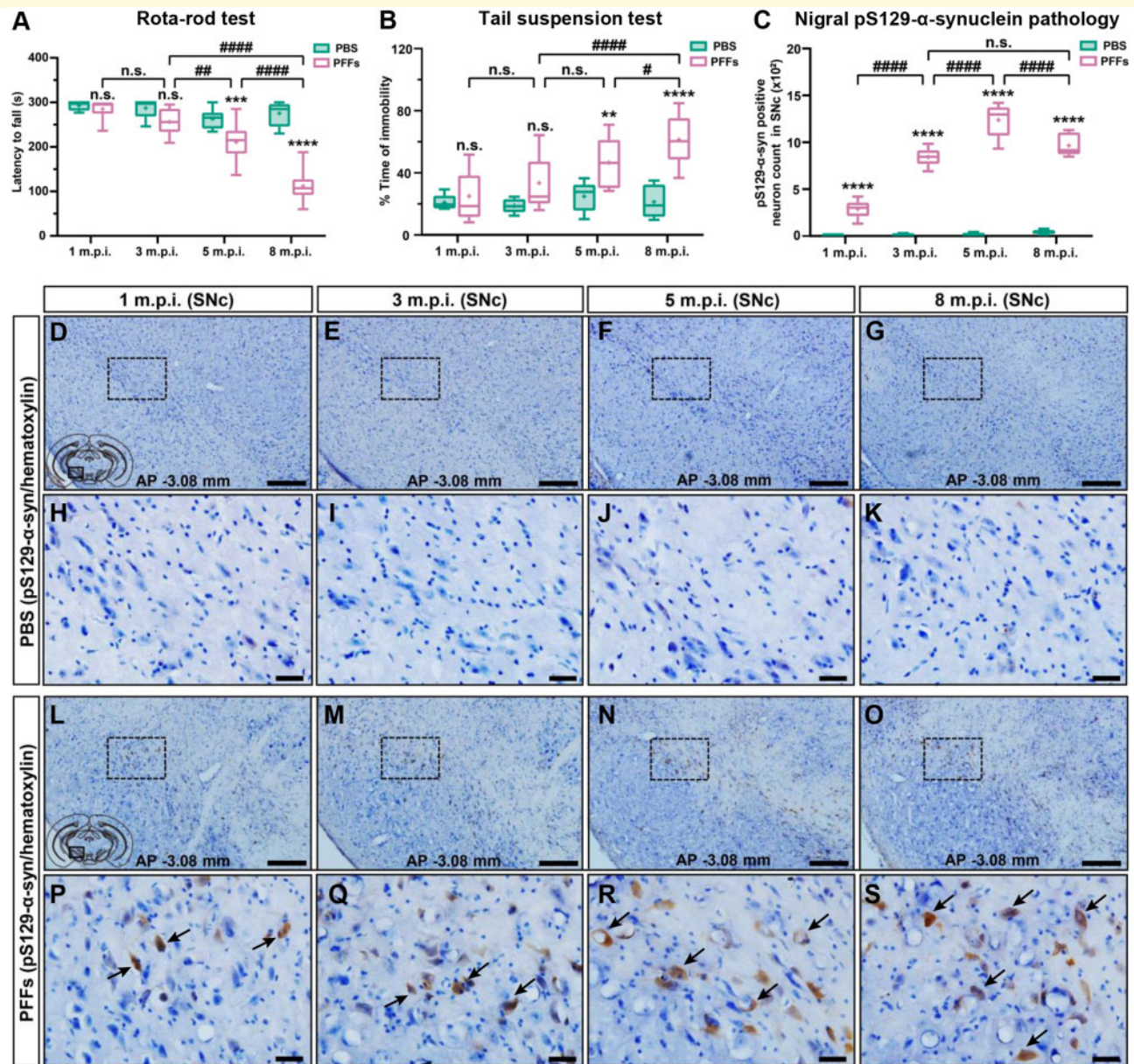


Figure 5 Progressive parkinsonian behavioural deficits and nigral α -synuclein pathology are identified in PFF-injected mice.

(A and B) Assessment and comparison of the locomotor dysfunction (A, rota-rod test) and depressive disorder (B, tail suspension test) between the PBS ($n = 5, 5, 8$ and 8) and PFFs ($n = 10, 10, 10$ and 20) mouse groups at 1, 3, 5 and 8 m.p.i. (C) Statistical comparison of the nigral pS129- α -synuclein-positive neuron quantities between PBS ($n = 5, 5, 5$ and 6) and PFFs ($n = 6, 6, 5$ and 7) mouse groups at 1, 3, 5 and 8 m.p.i. (D–S) Representative photomicrographs showing the pS129- α -synuclein immunostaining (indicated by arrows) in the SNc (AP -3.08 mm) of the PBS (D–G) and PFFs (L–O) mouse groups at 1, 3, 5 and 8 m.p.i., respectively. (H–K and P–S) Higher magnifications, respectively, of the rectangular areas in D–G and L–O. Scale bars = 200 μ m in D–G and L–O; 30 μ m in H–K and P–S. Box-and-whisker plots (A–C) show the means (plus sign), median, the 25th and 75th percentiles, minima and maxima. Statistical significance was determined using two-way ANOVA followed by Bonferroni's multiple comparison test. ** $P < 0.01$, *** $P < 0.001$, **** $P < 0.0001$ versus PBS group; # $P < 0.05$, ### $P < 0.01$, #### $P < 0.0001$, n.s. = not significant. pS129- α -syn = pS129- α -synuclein.

(Fig. 1) and, as a result, recapitulated typical RBD-like behaviours in mice (Fig. 2). This was consistent with previous RBD modelling study findings that manipulative neurochemical lesion (Lu *et al.*, 2006) or genetic incapacitation (Krenzer *et al.*, 2011; Valencia Garcia *et al.*, 2017)

of the SLD neurons can induce REM sleep without atonia (RWA) or RBD-like behaviours in rodents.

Following the functional verification of the SLD nucleus, we injected PFFs into this nucleus and established an α -synucleinopathy-based RBD mouse model via the seeding-

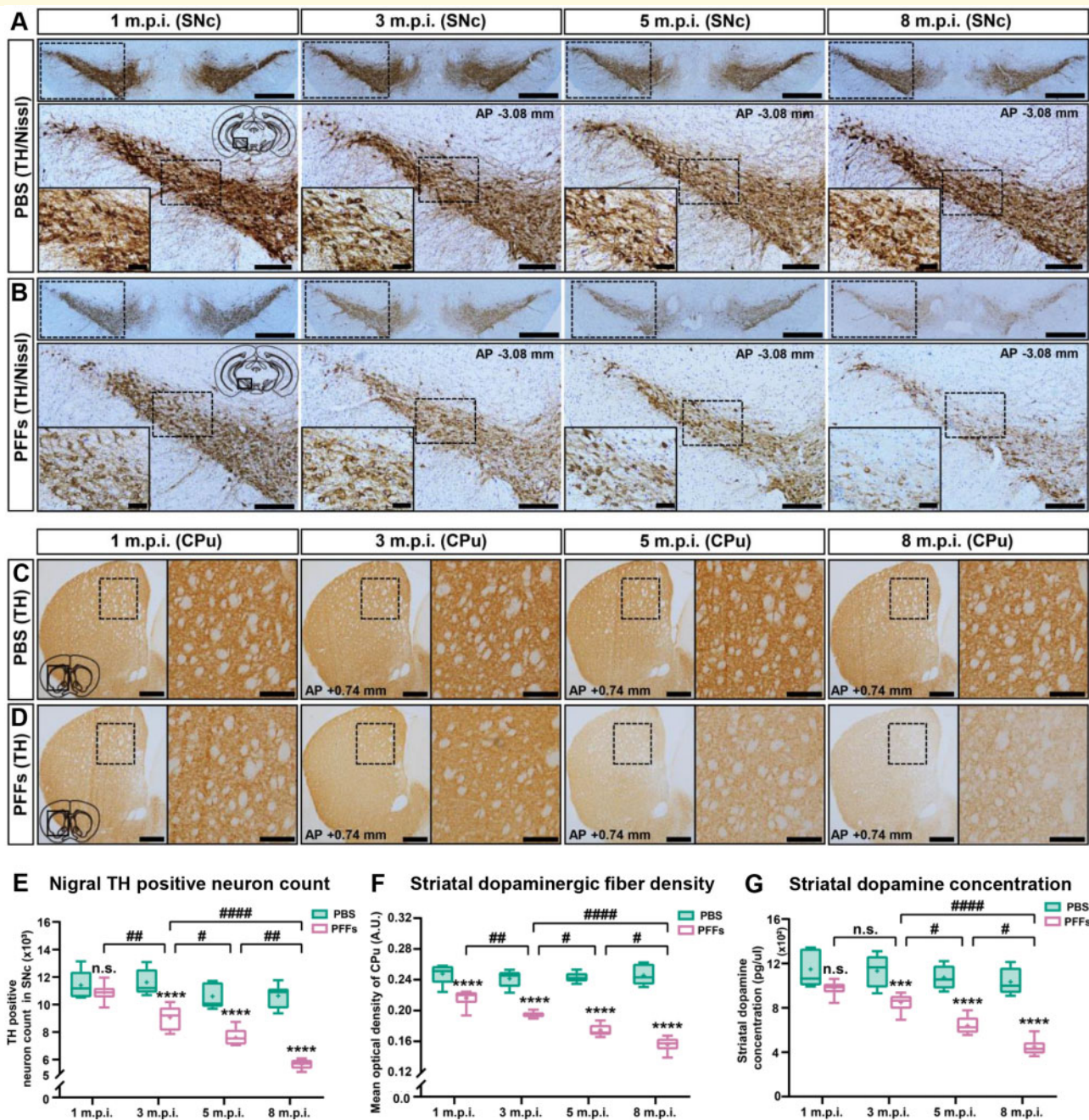


Figure 6 Progressive nigrostriatal dopaminergic neuron degeneration is identified in the PFF-injected mice. (A–D) Representative photomicrographs showing TH immunostaining in the SNc (A and B, AP –3.08 mm) and caudate putamen (C and D, AP +0.74 mm) of mice in the PBS (A and C) and PFFs (B and D) group at 1, 3, 5 and 8 m.p.i., respectively. The insets represent a higher magnification of the rectangular areas. (E–G) Statistical comparison of the nigral TH-positive neuron count (E), striatal dopaminergic fibre density (F) and striatal dopamine concentration (G) between PBS ($n = 5, 5, 5$ and 6) and PFFs ($n = 6, 6, 5$ and 7) groups at 1, 3, 5 and 8 m.p.i., respectively. Scale bars = 1 mm for A and B (top panels); 500 μm for C and D (left panels); 200 μm for A and B (bottom panels), C and D (right panels); 50 μm for the insets of A–D. Box-and-whisker plots (E–G) showed the means (plus sign), median, the 25th and 75th percentiles, minima and maxima. Statistical significance was determined using two-way ANOVA followed by Bonferroni's multiple comparison test. $***p < 0.001$, $****p < 0.0001$ versus PBS group; $\#p < 0.05$, $##p < 0.01$, $####p < 0.0001$, n.s. = not significant. A.U. = arbitrary unit; CPu = caudate putamen.

propagation property of PFFs (Lee et al., 2010; Masuda-Suzukake et al., 2013; Volpicelli-Daley et al., 2014; Karpowicz et al., 2019). Unlike previous RBD animal models that are based on the mechanical destruction (Jouvet,

1962), neurotoxic lesion (Lu et al., 2006) or genetic inactivation (Krenzer et al., 2011; Valencia Garcia et al., 2017, 2018) of the REM sleep circuit, this RBD mouse model was established based on α -synucleinopathy-induced neuron

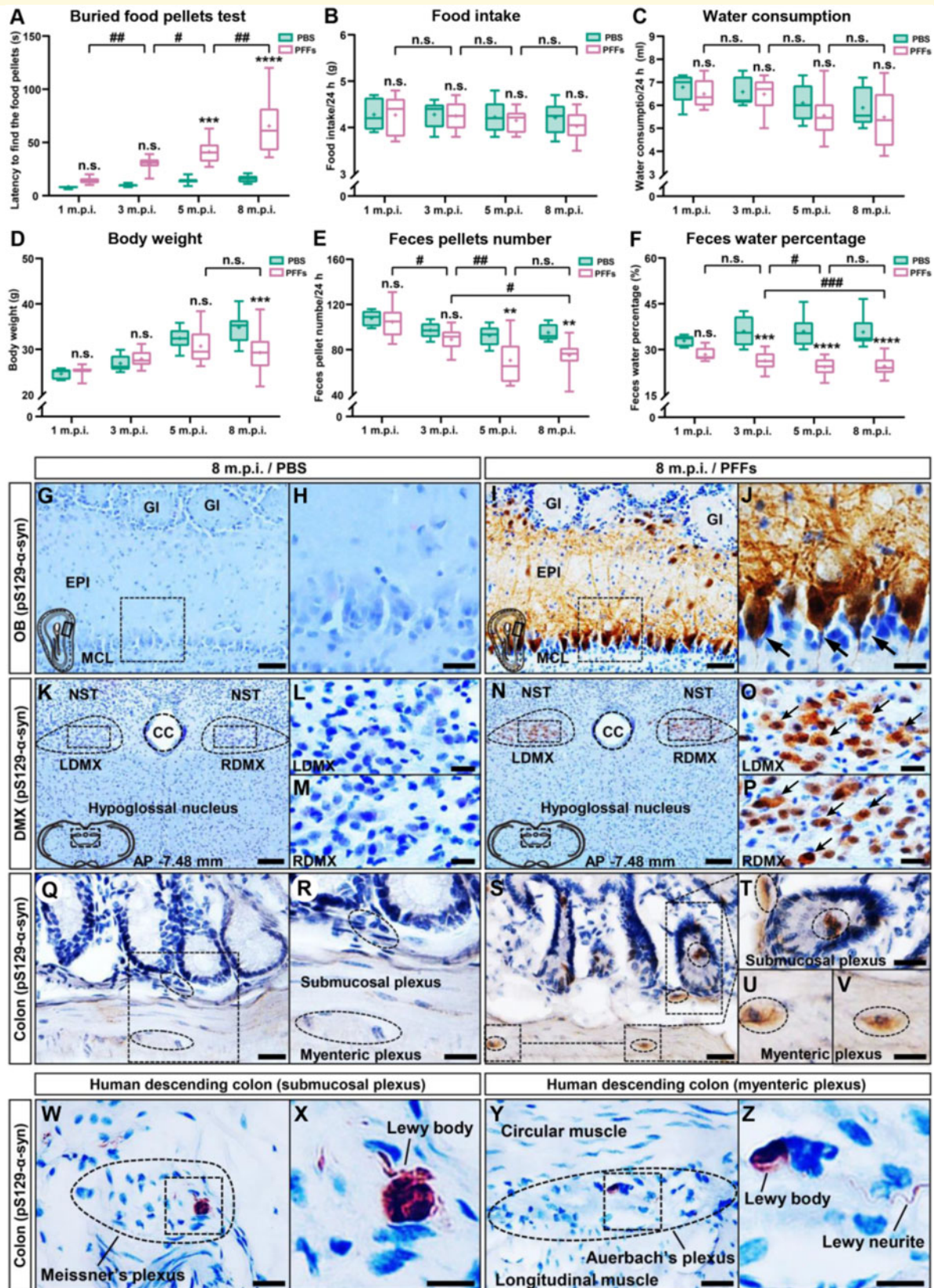


Figure 7 Seeded α -synuclein pathology underlies the olfactory dysfunction and gastrointestinal dysmotility in PFF-injected mice. (A) Assessment and comparison of the olfaction between the PBS ($n = 5, 5, 8$ and 8) and PFFs ($n = 10, 10, 10$ and 20) mouse groups at 1, 3, 5 and 8 m.p.i. (B–F) Gastrointestinal motility function of the PBS ($n = 5, 5, 8$ and 8) and PFFs ($n = 10, 10, 10$ and 20) group mice was assessed with the following five indicators: food intake/24 h (B), water consumption/24 h (C), body weight (D), faecal pellets number/24 h (E) and faecal water percentage (F). (G–V) Representative photomicrographs showing the pS129- α -synuclein immunostaining (indicated by arrows) in the OB

(continued)

degeneration within SLD, which could therefore represent the pathophysiological basis of idiopathic RBD in humans (Fifel et al., 2016; Hogg et al., 2018). A recent study reported that heterozygous A53T SNCA bacterial artificial chromosome (BAC) transgenic mice display age-dependent increase of REM/SWS EMG variance ratio (Taguchi et al., 2019), which was reminiscent of RWA in RBD patients. Moreover, phosphorylated α -synuclein pathology are also identified in the RBD-related brain subregions such as SLD, pedunculo-pontine tegmental nucleus and alpha gigantocellular nucleus (Taguchi et al., 2019). These histopathological findings suggested that this transgenic RBD mouse model was also characterized by α -synucleinopathy, but it lacked the neuron degeneration evidences within the RBD-related regions, e.g., SLD. Given this, we determined the SLD neuron quantities in this study (Fig. 4), and further proved that it was negatively correlated with the RBD behaviours (Supplementary Fig. 10). Based on this evidence, we demonstrated that the PFF-seeded α -synucleinopathy and resultant SLD neuron degeneration could underlie the RBD behaviours in mice.

As recommended by the ICSD-3 (International Classification of Sleep Disorders, 3rd edition), clinical diagnosis of RBD is based on either dream enactment behaviours or polysomnographic evidence of RWA (Sateia, 2014). To describe the characteristic of myoelectric bursts during REM sleep, RWA is further categorized into two subtypes: tonic and phasic RWA (Lapierre and Montplaisir, 1992; Postuma et al., 2010). In comparison with the phasic RWA, tonic RWA usually manifests as continuous muscle tonus (Lapierre and Montplaisir, 1992; Postuma et al., 2010). These two types of RWA are proven to be correlated with different pontomedullary structures (Postuma et al., 2010; Iranzo, 2018; Liu et al., 2019). Phasic RWA is supposed to result from the dysfunction of motor cortex and ventromedial medulla (Boeve et al., 2007b; Postuma et al., 2010; Valencia Garcia et al., 2018; Sunwoo et al., 2019), while tonic RWA is considered to be correlated with the neuron degeneration within SLD (Boeve et al., 2007b; Postuma et al., 2010; Boeve, 2013; Peever et al., 2014; McKenna and Peever, 2017; Liu et al., 2019). In line with these previous findings, we identified in this study that the injection of PFFs into SLD could induce frequent myoelectric bursts and muscle tonus during REM sleep (Fig. 3B, D and F), which mimicked the polysomnographic features of tonic RWA

(Sateia, 2014; Dijkstra et al., 2019). Moreover, further quantitative analysis revealed significantly elevated muscle tone intensity during REM sleep (EMG_{REM}) in this RBD mouse model (Fig. 3H), which was also consistent with the increased muscle tonus identified in tonic RWA (Sateia, 2014).

Increasing *in vivo* and *in vitro* studies demonstrate that PFFs can induce the formation and transmission of α -synucleinopathy by seeding endogenous soluble α -synuclein to form insoluble pathological aggregates (Luk et al., 2009, 2012a, b; Volpicelli-Daley et al., 2014). In particular, when injecting PFFs into the olfactory bulb or enteral neuroplexus, the PFF-seeded α -synuclein pathology not only recapitulates hyposmia (Rey et al., 2016) and gastrointestinal dysmotility (Kim et al., 2019), but also models Parkinson's disease-like neurodegeneration in mice (Kim et al., 2019). Similar to that, we demonstrated in this study that injection of PFFs into the SLD could induce RBD-like behaviours in mice and thus established an α -synucleinopathy-based RBD mouse model. Nevertheless, unlike previously reported RBD animal models (Jouvet, 1962; Lu et al., 2006; Krenzer et al., 2011; Valencia Garcia et al., 2017, 2018), this novel mouse model was not stationary, which could continuously progress to develop nigrostriatal degeneration and parkinsonian behavioural deficits (Figs 5 and 6). During this phenoconversion process, we identified widespread and time-dependent aggregation of α -synuclein pathology in a wide range of brain structures, which extended from the rostral olfactory bulb to caudal vagal nucleus (Supplementary Fig. 13) and even involved the peripheral enteral neuroplexuses (Fig. 7S). These neuropathological data could underlie the progressive parkinsonian behavioural deficits and neurodegenerations determined in the mice. Hence, we, for the first time, recapitulated parkinsonian behavioural and histopathological phenotypes in an α -synucleinopathy-based RBD animal model, which provided experimental supporting evidences for the clinical phenoconversion of RBD to parkinsonian disorders (Schenck et al., 1996, 2013; Iranzo et al., 2013, 2014; Postuma et al., 2019).

The recently reported A53T-SNCA transgenic RBD mouse model was proven to express pathological forms of α -synuclein in several Parkinson's disease-related brain regions, but it did not replicate any parkinsonian locomotor dysfunctions throughout the experimental period (Taguchi et al., 2019).

Figure 7 Continued

(G–J), DMX (K–P) and colon (Q–V, AP –7.48 mm) of PBS (8 m.p.i.) and PFFs (8 m.p.i.) group mice. (W–Z) Photomicrographs showing the pS129- α -synuclein immunostaining in the patient's colonic neuroplexus: submucosal plexus (Meissner's plexus; W and X; indicated by circles) and myenteric plexus (Auerbach's plexus; Y and Z; indicated by circles). H, J, L, M, O, P, R, T, U, V, X and Z are a higher magnification of the rectangular areas in the corresponding left panel images. Scale bars = 100 μ m in K and N; 50 μ m in G, I, Q, S, X and Z; 30 μ m in W and Y; 20 μ m in H, J, R, T, U and V; 10 μ m in L, M, O and P. Box-and-whisker plots (A–F) show the means (plus sign), median, the 25th and 75th percentiles, minima and maxima. Statistical significance was determined using two-way ANOVA followed by Bonferroni's multiple comparison test. ** $P < 0.01$, *** $P < 0.001$, **** $P < 0.0001$ versus PBS group; # $P < 0.05$, ## $P < 0.01$, ### $P < 0.001$, n.s. = not significant. cc = central canal; EPI = external plexiform layer of olfactory bulb; Gl = glomerular layer of olfactory bulb; L/RDMX = left/right dorsal motor nucleus of vagus nerve; MCL = mitral cell layer of olfactory bulb; NST = nucleus of solitary tract; pS129- α -syn = pS129- α -synuclein.

As we know, the motor symptoms in patients with Parkinson's disease only manifest when there is a substantial degeneration (e.g. 50% dopaminergic neuron loss, 60–80% striatal dopamine depletion) of the nigrostriatal system (Bezard *et al.*, 2003). In this transgenic mouse model, although the dopaminergic neuron number decreased in an age-dependent manner, 17.1% of the neurons degenerated by the age of 18 months. The striatal TH expression and dopamine content remain unaltered throughout the experiment (Taguchi *et al.*, 2019). This was in contrast with the striatal dopamine depletion, dopaminergic fibre denervation and locomotor dysfunction that identified in our mouse model. The most prominent difference between these two animal models was that the former was established on the A53T-SNCA transgenic background and the latter on PFF injection. Previous studies suggest that artificial gene editing in α -synuclein transgenic mice can induce adaptive gene expression profile changes and this may confer neuroprotective effects (Itier *et al.*, 2003; Dawson *et al.*, 2010). Besides, compensatory mechanisms can also be initiated to postpone the dopaminergic neuron degeneration and prevent the motor dysfunctions in the transgenic mouse model (Bezard *et al.*, 2003; Palop *et al.*, 2006; Dawson *et al.*, 2010). In comparison, the prion-like seeding property of PFFs (Lee *et al.*, 2010; Masuda-Suzukake *et al.*, 2013; Volpicelli-Daley *et al.*, 2014; Karpowicz *et al.*, 2019) enabled the α -synucleinopathy-based mouse model break through the compensation threshold, which contributed to progressive nigrostriatal degeneration and parkinsonian behavioural dysfunction.

Extensive clinical and neuropathological evidences indicate that Parkinson's disease is a global neurodegeneration disorder, with degeneration implicating both the central and peripheral nervous system (Poewe *et al.*, 2017; Schapira *et al.*, 2017). In this study, apart from the RBD and parkinsonian locomotor dysfunction, we demonstrated that the PFF-injected mice also displayed progressive olfactory dysfunction and gastrointestinal dysmotility (Fig. 7A–F), which could be attributed to the α -synucleinopathy accumulated in the olfactory bulb (Rey *et al.*, 2016) and vagal nucleus (Kim *et al.*, 2019; Challis *et al.*, 2020). Interestingly, we also identified pS129- α -synuclein aggregates in the submucosal and myenteric plexus of colon, and these evidences suggested a potential brain-to-gut transmission pattern of α -synuclein pathology. Nevertheless, this supposed transmission pattern was contrary to the well-recognized gut-to-brain propagation mode of α -synucleinopathy (Braak *et al.*, 2003). A recent study provided supporting evidences for this brain-to-gut transmission mode by demonstrating that α -synuclein can transfer from the central midbrain to peripheral stomach, with the dorsal motor nucleus of vagus nerve acting as the relay station and the efferent vagal visceromotor fibres as the conduits (Ulusoy *et al.*, 2017). In addition, several neural circuit tracing studies also demonstrate that there are direct monosynaptic fibre connections between the gut and brain (Han *et al.*, 2018; Kaelberer *et al.*, 2018), which could act as the transmission passage of α -synucleinopathy in pathological conditions. Based on these study findings and

observations, we supposed that there might exist bidirectional trans-synaptic transmission of α -synuclein pathology between the brain and gut, which has been confirmed by two very recent studies (Van Den Berge *et al.*, 2019; Marie-Laure *et al.*, 2020). In a transgenic BAC rat model, Van Den Berge *et al.* (2019) demonstrate bidirectional α -synucleinopathy propagation via the vagus nerve, i.e. duodenum–vagus nerve–brainstem–vagus nerve–stomach. While Marie-Laure *et al.* (2020) show that patient-derived α -synuclein aggregates can induce nigrostriatal degeneration and enteral nervous system pathology after either enteric or striatal injection in non-human primates, thus revealing bidirectional gut-to-brain and gut-to-brain propagation modes of synucleinopathy.

In summary, we introduced a novel α -synucleinopathy-based RBD mouse modelling strategy in this study and further demonstrated that the propagated α -synuclein pathology could recapitulate the phenoconversion of RBD to Parkinson's disease in this animal model (Supplementary Fig. 16). Additionally, our findings also added supporting evidences for the newly proposed bidirectional transmission pattern of α -synucleinopathy between gut and brain. In future studies, this novel animal model could not only help to unravel the mechanisms behind the initiation and phenoconversion of RBD, but also be used to develop or screen the disease-modifying therapeutics for Parkinson's disease.

Acknowledgements

We thank Xueyan Cao for her kindly assistance of performing the transmission electron microscopy analysis, and Jichuan Zhou, Yudong Yan, Zeka Chen, Han Guo and Huanying Shi for their help to perform the polysomnographic recordings. Many thanks to the editors and the two anonymous reviewers for their valuable comments and suggestions.

Funding

This study was supported by the grants (81571232, 81771372, 91949118, 81971194, 81701250, 81801260) from the National Natural Science Foundation of China, the projects (2016YFC1306500, 2016YFC1306504) from the Ministry of Science and Technology of China, and the Shanghai Municipal Science and Technology Major Project (No.2018SHZDZX01, No.2017SHZDZX01) and ZHANGJIANG LAB.

Competing interests

The authors report no competing interests.

Supplementary material

Supplementary material is available at *Brain* online.

References

- Bezard E, Gross CE, Brotchie JM. Presymptomatic compensation in Parkinson's disease is not dopamine-mediated. *Trends Neurosci* 2003; 26: 215–21.
- Boeve BF. Idiopathic REM sleep behaviour disorder in the development of Parkinson's disease. *Lancet Neurol* 2013; 12: 469–82.
- Boeve BF, Dickson DW, Olson EJ, Shepard JW, Silber MH, Ferman TJ, et al. Insights into REM sleep behavior disorder pathophysiology in brainstem-predominant Lewy body disease. *Sleep Med* 2007a; 8: 60–4.
- Boeve BF, Silber MH, Saper CB, Ferman TJ, Dickson DW, Parisi JE, et al. Pathophysiology of REM sleep behaviour disorder and relevance to neurodegenerative disease. *Brain* 2007b; 130: 2770–88.
- Braak H, Del Tredici K, Rub U, de Vos RA, Jansen Steur EN, Braak E. Staging of brain pathology related to sporadic Parkinson's disease. *Neurobiol Aging* 2003; 24: 197–211.
- Challis C, Hori A, Sampson TR, Yoo BB, Challis RC, Hamilton AM, et al. Gut-seeded alpha-synuclein fibrils promote gut dysfunction and brain pathology specifically in aged mice. *Nat Neurosci* 2020.
- Clement O, Sapin E, Berod A, Fort P, Luppi PH. Evidence that neurons of the sublaterodorsal tegmental nucleus triggering paradoxical (REM) sleep are glutamatergic. *Sleep* 2011; 34: 419–23.
- Dauvilliers Y, Schenck CH, Postuma RB, Iranzo A, Luppi PH, Plazzi G, et al. REM sleep behaviour disorder. *Nat Rev Dis Primers* 2018; 4: 19.
- Dawson TM, Ko HS, Dawson VL. Genetic animal models of Parkinson's disease. *Neuron* 2010; 66: 646–61.
- Dement W, Kleitman N. Cyclic variations in EEG during sleep and their relation to eye movements, body motility, and dreaming. *Electroencephalogr Clin Neurophysiol* 1957; 9: 673–90.
- Desplats P, Lee H, Bae E, Patrick C, Rockenstein E, Crews L, et al. Inclusion formation and neuronal cell death through neuron-to-neuron transmission of alpha-synuclein. *Proc Natl Acad Sci U S A* 2009; 106: 13010–5.
- Dijkstra F, Viaene M, Crosiers D, De Volder I, Cras P. Frequency and characteristic features of REM sleep without atonia. *Clin Neurophysiol* 2019; 130: 1825–32.
- Fifel K, Piggins H, Deboer T. Modeling sleep alterations in Parkinson's disease: how close are we to valid translational animal models? *Sleep Med Rev* 2016; 25: 95–111.
- Fort P, Bassetti CL, Luppi PH. Alternating vigilance states: new insights regarding neuronal networks and mechanisms. *Eur J Neurosci* 2009; 29: 1741–53.
- Franklin KBJ, Paxinos G, Paxinos and Franklin's The mouse brain in stereotaxic coordinates. 3rd edn. Amsterdam: Academic Press; 2013.
- Fuller PM, Saper CB, Lu J. The pontine REM switch: past and present. *J Physiol* 2007; 584: 735–41.
- Han W, Tellez LA, Perkins MH, Perez IO, Qu T, Ferreira J, et al. A neural circuit for gut-induced reward. *Cell* 2018; 175: 887–8.
- Hogel B, Stefani A, Videnovic A. Idiopathic REM sleep behaviour disorder and neurodegeneration - an update. *Nat Rev Neurol* 2018; 14: 40–55.
- Iranzo A. The REM sleep circuit and how its impairment leads to REM sleep behavior disorder. *Cell Tissue Res* 2018; 373: 245–66.
- Iranzo A, Fernandez-Arcos A, Tolosa E, Serradell M, Molinuevo JL, Valldeoriola F, et al. Neurodegenerative disorder risk in idiopathic REM sleep behavior disorder: study in 174 patients. *PLoS One* 2014; 9: e89741.
- Iranzo A, Tolosa E, Gelpi E, Molinuevo JL, Valldeoriola F, Serradell M, et al. Neurodegenerative disease status and post-mortem pathology in idiopathic rapid-eye-movement sleep behaviour disorder: an observational cohort study. *Lancet Neurol* 2013; 12: 443–53.
- Itier JM, Ibanez P, Mena MA, Abbas N, Cohen-Salmon C, Bohme GA, et al. Parkin gene inactivation alters behaviour and dopamine neurotransmission in the mouse. *Hum Mol Genet* 2003; 12: 2277–91.
- Jouvet M. Recherches sur les structures nerveuses et les mécanismes responsables des différentes phases du sommeil physiologique. *Arch. Ital. Biol* 1962; 100: 125–206.
- Kaelberer MM, Buchanan KL, Klein ME, Barth BB, Montoya MM, Shen X, et al. A gut-brain neural circuit for nutrient sensory transduction. *Science* 2018; 361.
- Karpowicz RJ, Jr., Trojanowski JQ, Lee VM. Transmission of alpha-synuclein seeds in neurodegenerative disease: recent developments. *Lab Invest* 2019; 99: 971–81.
- Kim S, Kwon SH, Kam TI, Panicker N, Karuppagounder SS, Lee S, et al. Transneuronal propagation of pathologic alpha-synuclein from the gut to the brain models Parkinson's disease. *Neuron* 2019; 103: 627–41 e7.
- Krenzer M, Anacleit C, Vetrivelan R, Wang N, Vong L, Lowell BB, et al. Brainstem and spinal cord circuitry regulating REM sleep and muscle atonia. *PLoS One* 2011; 6: e24998.
- Lapierre O, Montplaisir J. Polysomnographic features of REM sleep behavior disorder: development of a scoring method. *Neurology* 1992; 42: 1371–4.
- Lee SJ, Desplats P, Sigurdson C, Tsigelny I, Masliah E. Cell-to-cell transmission of non-prion protein aggregates. *Nat Rev Neurol* 2010; 6: 702–6.
- Liu Y, Zhang J, Lam SP, Yu MWM, Li SX, Zhou J, et al. Electromyography activity level in rapid eye movement sleep predicts neurodegenerative diseases in idiopathic rapid eye movement sleep behavior disorder: a 5-year longitudinal study. *Sleep Med* 2019; 56: 128–34.
- Lu J, Sherman D, Devor M, Saper CB. A putative flip-flop switch for control of REM sleep. *Nature* 2006; 441: 589–94.
- Luk KC, Kehm V, Carroll J, Zhang B, O'Brien P, Trojanowski JQ, et al. Pathological alpha-synuclein transmission initiates Parkinson-like neurodegeneration in nontransgenic mice. *Science* 2012a; 338: 949–53.
- Luk KC, Kehm VM, Zhang B, O'Brien P, Trojanowski JQ, Lee VM. Intracerebral inoculation of pathological alpha-synuclein initiates a rapidly progressive neurodegenerative alpha-synucleinopathy in mice. *J Exp Med* 2012b; 209: 975–86.
- Luk KC, Song C, O'Brien P, Stieber A, Branch JR, Brunden KR, et al. Exogenous α -synuclein fibrils seed the formation of Lewy body-like intracellular inclusions in cultured cells. *Proc Natl Acad Sci U S A* 2009; 106: 20051–6.
- Luppi PH, Clement O, Sapin E, Gervasoni D, Peyron C, Leger L, et al. The neuronal network responsible for paradoxical sleep and its dysfunctions causing narcolepsy and rapid eye movement (REM) behavior disorder. *Sleep Med Rev* 2011; 15: 153–63.
- Marie-Laure A, Sandra D, Alice P, Mathieu B, Sandrine C, Gregory P, et al. Bidirectional gut-to-brain and brain-to-gut propagation of synucleinopathy in non-human primates. *Brain* 2020; 143: 1462–75.
- Mao X, Ou MT, Karuppagounder SS, Kam T, Yin X, Xiong Y, et al. Pathological α -synuclein transmission initiated by binding lymphocyte-activation gene 3. *Science* 2016; 353: aah3374.
- Masuda-Suzukake M, Nonaka T, Hosokawa M, Oikawa T, Arai T, Akiyama H, et al. Prion-like spreading of pathological alpha-synuclein in brain. *Brain* 2013; 136: 1128–38.
- McKenna D, Peever J. Degeneration of rapid eye movement sleep circuitry underlies rapid eye movement sleep behavior disorder. *Mov Disord* 2017; 32: 636–44.
- Moore HM, Kelly AB, Jewell SD, McShane LM, Clark DP, Greenspan R, et al. Biospecimen reporting for improved study quality (BRISQ). *Cancer Cytopathol* 2011; 119: 92–101.
- Palop JJ, Chin J, Mucke L. A network dysfunction perspective on neurodegenerative diseases. *Nature* 2006; 443: 768–73.
- Peever J, Luppi PH, Montplaisir J. Breakdown in REM sleep circuitry underlies REM sleep behavior disorder. *Trends Neurosci* 2014; 37: 279–88.
- Peever J, Fuller PM. The biology of REM sleep. *Curr Biol* 2017; 27: R1237–48.

- Poewe W, Seppi K, Tanner CM, Halliday GM, Brundin P, Volkman J, et al. Parkinson disease. *Nat Rev Dis Primers* 2017; 3: 17013.
- Postuma RB, Gagnon JF, Rompre S, Montplaisir JY. Severity of REM atonia loss in idiopathic REM sleep behavior disorder predicts Parkinson disease. *Neurology* 2010; 74: 239–44.
- Postuma RB, Iranzo A, Hu M, Hogg B, Boeve BF, Manni R, et al. Risk and predictors of dementia and parkinsonism in idiopathic REM sleep behaviour disorder: a multicentre study. *Brain* 2019; 142: 744–59.
- Rey NL, Steiner JA, Maroof N, Luk KC, Madaj Z, Trojanowski JQ, et al. Widespread transneuronal propagation of alpha-synucleinopathy triggered in olfactory bulb mimics prodromal Parkinson's disease. *J Exp Med* 2016; 213: 1759–78.
- Sateia MJ. International classification of sleep disorders-third edition: highlights and modifications. *Chest* 2014; 146: 1387–94.
- Schapiro AHV, Chaudhuri KR, Jenner P. Non-motor features of Parkinson disease. *Nat Rev Neurosci* 2017; 18: 509.
- Schenck CH, Boeve BF, Mahowald MW. Delayed emergence of a parkinsonian disorder or dementia in 81% of older men initially diagnosed with idiopathic rapid eye movement sleep behavior disorder: a 16-year update on a previously reported series. *Sleep Med* 2013; 14: 744–8.
- Schenck CH, Bundlie SR, Ettinger MG, Mahowald MW. Chronic behavioral disorders of human REM sleep: a new category of parasomnia. *Sleep* 1986; 9: 293–308.
- Schenck CH, Bundlie SR, Mahowald MW. Delayed emergence of a parkinsonian disorder in 38% of 29 older men initially diagnosed with idiopathic rapid eye movement sleep behaviour disorder. *Neurology* 1996; 46: 388–93.
- Sunwoo JS, Cha KS, Byun JI, Kim TJ, Jun JS, Lim JA, et al. Abnormal activation of motor cortical network during phasic REM sleep in idiopathic REM sleep behavior disorder. *Sleep* 2019; 42: zsy227.
- Taguchi T, Ikuno M, Hondo M, Parajuli L K, Taguchi K, Ueda J, et al. α -Synuclein BAC transgenic mice exhibit RBD-like behaviour and hyposmia: a prodromal Parkinson's disease model. *Brain* 2020; 143: 249–65.
- Turner RS, D'Amato CJ, Chervin RD, Blaivas M. The pathology of REM sleep behavior disorder with comorbid Lewy body dementia. *Neurology* 2000; 55: 1730–2.
- Uchiyama M, Isse K, Tanaka K, Yokota N, Hamamoto M, Aida S, et al. Incidental Lewy body disease in a patient with REM sleep behavior disorder. *Neurology* 1995; 45: 709–12.
- Ulusoy A, Phillips RJ, Helwig M, Klinkenberg M, Powley TL, Di Monte DA. Brain-to-stomach transfer of alpha-synuclein via vagal preganglionic projections. *Acta Neuropathol* 2017; 133: 381–93.
- Valencia Garcia S, Brischoux F, Clement O, Libourel PA, Arthaud S, Lazarus M, et al. Ventromedial medulla inhibitory neuron inactivation induces REM sleep without atonia and REM sleep behavior disorder. *Nat Commun* 2018; 9: 504.
- Valencia Garcia S, Libourel PA, Lazarus M, Grassi D, Luppi PH, Fort P. Genetic inactivation of glutamate neurons in the rat sublaterodorsal tegmental nucleus recapitulates REM sleep behaviour disorder. *Brain* 2017; 140: 414–28.
- Van Den Berge N, Ferreira N, Gram H, Mikkelsen TW, Alstrup AKO, Casadei N, et al. Evidence for bidirectional and trans-synaptic parasympathetic and sympathetic propagation of alpha-synuclein in rats. *Acta Neuropathol* 2019; 138: 535–50.
- Volpicelli-Daley LA, Luk KC, Lee VM. Addition of exogenous alpha-synuclein preformed fibrils to primary neuronal cultures to seed recruitment of endogenous alpha-synuclein to Lewy body and Lewy neurite-like aggregates. *Nat Protoc* 2014; 9: 2135–46.
- Weil RS, Morris HR. REM sleep behaviour disorder: an early window for prevention in neurodegeneration? *Brain* 2019; 142: 498–501.
- Xue WF, Hellewell AL, Gosal WS, Homans SW, Hewitt EW, Radford SE. Fibril fragmentation enhances amyloid cytotoxicity. *J Biol Chem* 2009; 284: 34272–82.
- Zhang Z, Wang HJ, Wang DR, Qu WM, Huang ZL. Red light at intensities above 10 lx alters sleep-wake behavior in mice. *Light Sci Appl* 2017; 6: e16231.